A Coupled Reactive Transport Model for the Simulation of Carbonate Dissolution During CO_2 Sequestration: Investigating the Effect of Pore-Size Distribution

Flor Wassing
(student number: 4163001)

MSc Thesis
Earth Surface and Water
University Utrecht
04-10-2019

First supervisor: dr. Amir Raoof
Second supervisor: prof. dr. Ruud Schotting

Abstract

In this research, a coupled chemical reactive transport model is developed for the simulation of calcite dissolution under CO_2 storage conditions. The coupled model is applied to systematically evaluate the relative effects of pore-structure parameters and their evolution during calcite dissolution. Pore-structures are represented using different pore networks which vary in pore-size distribution and average pore connectivity (i.e. coordination number). The model discretises the 3D pore-network generated using PoreFlow software into several cells over which PHREEQC performs 1D reactive transport calculations. Through averaging, PoreFlow outputs the pore-throat radii and total specific reactive surface area for each cell, which is needed for the reaction calculations using PHREEQC. Subsequently, PHREEQC outputs the calculated amount of dissolved calcite for PoreFlow where it is redistributed over the network according to the relative residence times of the various pore-throats. For simplicity it is assumed that dissolution only occurs within pore-throats and that pores with a shorter residence time dissolve more than pores with a longer residence time. Through this coupling, reactive transport calculations can be done at a relatively low computational cost whilst still taking into account the evolution of pore-structure. Results of reactive transport simulations indicated a relatively high reactivity which can be attributed to the high temperature and pressure conditions but could also be caused by an overestimation of the rate considering the system may not be well-mixed for the velocity used. Notably, the average coordination number is found to have a negligible effect on the evolution of the pore-throat radius distribution. Furthermore, networks with a small mean pore-size are found to be much more sensitive to dissolution and show more drastic variations for changes in standard deviation. This may be attributed to small pores increasing at a much faster rate than large pores. Moreover, because pore networks with a smaller mean pore-size have a higher density of pores they will also have relatively more reactive surface area and will thus dissolve faster than networks with a higher mean pore-size. The relationship between residence time and pore-throat radius is shown to be insufficient to explain the observed evolution of pore-throat distribution and thus gives further evidence of the complexity of the system.

Contents

1 Introduction

In recent centuries anthropogenic CO_2 emissions have rapidly increased and predictions suggest that, with the growing global population and the associated growing energy demand, the CO_2 concentrations in the atmosphere will continue to rise in the future unless a drastic reduction of CO_2 emissions is implemented [Ramharack et al 2010]. A major concern is that the anthropogenic CO_2 and other greenhouse gas emissions are producing an enhanced greenhouse effect in the Earth's atmosphere, which is resulting in global warming [Stocker and Schmittner, 1997][T.J. Crowley, 1999][Solomon et al. 2009][IPCC, 2013]. CO_2 sequestration, the capture and long-term storage of anthropogenic CO_2 in the subsurface, is gaining interest as a possible solution to stabilize and reduce the concentration of CO_2 in the atmosphere. The primary challenge is ensuring that the CO_2 remains securely stored underground for a significant amount of time (hundreds to thousands of years) so that it can no longer contribute to climate change. Potential storage sites such as depleted oil and gas reservoirs [Kovscek and Wang, 2005] and deep saline aquifers [Bachu et al. 2003], are often composed of carbonate rock or sandstone that contains some degree of carbonate minerals as a cement fraction. When the injected CO_2 dissolves into the formation water it forms a weak acid, which will then react with the carbonate minerals in the surrounding host rock, leading to mineral dissolution and precipitation reactions. The precipitation of carbonate minerals is a form of CO_2 immobilization, which is referred to in literature as mineral trapping [Gunter et al. 1996]. The reverse dissolution reaction, however, is problematic for CO_2 storage as it could corrode the formation or overlying cap rock and thus create pathways through which CO_2 can escape back to the surface. The behaviour of these chemical reactions is dependent on various factors such as the composition of the fluid, the composition of the host rock, flow rates and in situ pressure and temperature [Rochelle et al, 2004]. It is further complicated by several feedback effects and the close coupling between chemical and physical processes. For instance, dissolution and precipitation reactions induce changes in pore-geometry which affect the porosity and permeability of the formation, resulting in changes in flow rates which in turn could affect the rate of dissolution/precipitation [e.g. Andreani et al. (2009)]. Moreover, the dissolution/precipitation reactions also affect the reactive surface area which again affects the reaction kinetics [e.g. Noiriel et al. (2009)]. Mineral dissolution and precipitation reactions can have significant consequences for the long-term storage security of CO_2 and thus a fundamental understanding of the rock-fluid interactions involved is essential before CO_2 storage can be proposed as a reliable option to mitigate CO_2 emissions in the atmosphere.

As it is very difficult to obtain enough qualitative and quantitative data through experiments alone, numerical modeling is a useful tool to investigate various coupled processes occurring during the reactive transport of CO_2 in the subsurface. Reactive transport processes are essentially all occurring at the pore-scale; however, it is not computationally feasible to perform such detailed modeling over the large spatial scales at which CO_2 storage is implemented. Typically, a continuum approach is used instead, where pore-scale properties are averaged over a macroscopic length scale and lumped together in various effective constitutive parameters such as porosity, permeability, dispersivity, tortuosity, and specific mineral surface area. However, because natural porous media is inherently heterogeneous, these parameters are scale-dependent which makes it difficult to find appropriate and representative values. Determination of these parameters is often based on empirical relationships that are limited in their detail and applicability. During reactive transport there is an added complication that the parameters are evolving in time due to the chemically induced changes in pore-geometry. Upscaling is also an important issue regarding reaction rates as they have been found to be scale dependent as well. Li et al. (2006) investigated several upscaling procedures for reactive transport at the pore-scale and demonstrated that continuum approaches or volume averaging approaches often introduce significant errors. This is because the rate laws that are used are often

measured in well-mixed laboratory systems, whereas porous media cannot always be considered well-mixed. While it is true that under certain flow conditions single pores may be considered well-mixed [Li et al., 2008], concentration gradients are still likely to develop at the network scale due to pore-scale heterogeneities and the effect of diffusion between pores [Li et al. 2006].

The importance of pore scale processes has become increasingly evident and has led to an increasing interest in pore-scale modeling of reactive transport in porous media. Modeling at this scale can be useful in gaining more insight in the scale-dependency of continuum parameters and their evolution during reactive transport. The relative impact of system properties can be easily investigated through systematic variation, something which is otherwise very difficult to achieve experimentally. A popular pore-scale modeling approach is pore network modeling (PNM), where a porous medium is represented as a network of pore bodies and pore throats of varying size, interconnected according to a specified topological configuration. The change in solute mass is calculated for each pore by using mass balance equations. While this idealization of pore space fails to capture any sub-pore gradients (i.e. each pore is typically assigned averaged values for concentration) it does allow for simulation over larger domain sizes (i.e. core-scale) at a relatively modest computational expense compared to other pore-scale modelling techniques such as the Lattice Boltzmann method.

Pore network modelling has been widely employed to investigate various reactive transport processes in porous media such as reaction-induced changes in transport properties [Algive et al. 2010, Varloteaux et al. 2013, Nogues et al. 2013], the scaling effect of adsorption [Raoof et al. 2010], upscaling of reaction rates [Li et al. 2006][Kim et al. 2011] and the response of wellbore cement during geological storage of CO_2 [Raoof et al. 2012]. While a lot of progress has been made in understanding the coupling between physical and chemical processes that occurs during reactive transport, many fundamental problems remain to be solved before accurate long-term prediction for CO_2 sequestration can be made. Pore-scale modeling has been proven a useful tool to simulate pore-scale processes and improve the understanding of the feedback mechanisms occurring at the continuum scale. However, it remains a challenge to upscale pore-network models for use in continuum models as they are still limited by the size of the network and will run into computational issues when solving for very large networks [Mehmani et al., 2012]. Another challenge is ensuring an accurate representation of the pore-structure, as it has major influence on flow properties and chemical reactions. Despite pore-network models using an idealized representation of pore-space, they are nevertheless capable of capturing important statistical characteristics such as pore-size distributions and coordination number distributions [e.g. Raoof et al., 2009]. These topological characteristics have been shown to be very important for the accurate representation of flow properties in porous media [Arns et al. 2004, Chatzis and Dullien, 1977]. However, knowledge on how these characteristics evolve during reactive transport and their relative impacts on flow properties and rate of reaction seems to be lacking.

The objective of this research is to develop an upscaled pore-network model which simulates pore-scale reactive transport of calcite dissolution under CO_2 storage conditions (high temperature and pressure). This is done by coupling PoreFlow [Raoof et al., 2013], a multi-directional pore-network (MDPN) model, with PHREEQC [Parkhurst and Appelo, 2013], a 1D reactive transport model, using a similar coupling method as proposed by Ameri et al. (2017). The basic concept behind this coupling method is that the pore-network properties in PoreFlow are upscaled such that 1D reactive transport calculations can be performed using PHREEQC, at relatively low computational cost. Because it is not intuitive what the relative effects are of the various pore-structure parameters or how they evolve during dissolution a systematic evaluation of pore-geometry is furthermore performed by running the model for several networks with varying pore-size distributions and average coordination numbers.

2 Background information

In this section a brief introduction is given to PoreFlow [Raoof et al., 2013] and PHREEQC [Parkhurst and Appelo, 2013], before discussing the coupled model approach in section 3 (*Methods)*.

2.1 PoreFlow

PoreFlow [Raoof et al., 2013] is a pore-network model capable of generating multi-directional pore-networks (MDPN) and simulating three-dimensional pore-scale fluid flow and solute transport in (variably) saturated porous media. PoreFlow represents a porous medium as a network of pore bodies that are connected by pore throats. A main feature of the model is that pore-throats can be oriented in 13 different directions, allowing for a maximum coordination number of 26 (Figure 1). With this wide range in coordination numbers, PoreFlow is then capable of generating a network with a specific coordination number distribution that matches that of a specific porous media. To further resemble a natural porous media structure, PoreFlow can also give pore throats a range of different cross-sectional shapes to account for the angularity found in real porous media. Further details on the network generation method can be found in Raoof and Hassanizadeh (2009).

To create a flow field across the network, PoreFlow imposes a pressure difference between the two opposing vertical boundaries and treats the boundaries parallel to the overall flow direction as no-flow boundaries. The discharge in any given pore throat is then calculate by the Hagen-Poiseuille equation:

$$q_{ij} = g_{ij}(p_j - p_i)\,, \tag{1}$$

where q_{ij} is the total volumetric flow rate [L^3T^{-1}] through the pore throat ij (connecting pore body i and j, see Fig. 1), g_{ij} is the conductance of pore throat ij [$L^3(ML^{-1}T^{-2})^{-1}T^{-1}$], and p_i and p_j are the fluid pressures [$ML^{-1}T^{-2}$] in pore bodies i and j, respectively. The conductance, g_{ij}, for a cylindrical pore throat is described by:

$$g_{ij} = \frac{\pi \cdot R_{ij}^4}{8 \cdot \mu \cdot l_{ij}}, \tag{2}$$

where R_{ij} is the pore throat radius [L], μ is the fluid dynamic viscosity [$(ML^{-1}T^{-2})$*T], and l_{ij} is the length [L] of the pore throat. Furthermore, for incompressible and steady-state flow, the continuity equation requires that the sum of discharges in and out of a pore body equal zero:

$$\sum_{j=1}^{z_i} q_{ij} = 0 \tag{3}$$

where z_i is the coordination number of pore body i. The above equation applies to all pore bodies in the network, except those lying at the flow boundaries where pressures are fixed.
By combining the above equations, the pore body pressures can be determined, after which Eq. 1 can be used to calculate the pore throat velocities (discharge divided by cross-sectional area) as well as the total discharge of the network Q_t. The total discharge is equal to the sum of fluxes through all the pore throats at the inlet and outlet of the boundary, and can subsequently be used to calculate the average pore velocity, $\bar{v}$, and permeability, k, of the network:

$$\bar{v} = \frac{Q_t \cdot L}{V_f}, \tag{4}$$

$$k = \frac{\mu \cdot Q_t \cdot L}{A \cdot \Delta P}, \tag{5}$$

L is the network length [L], V_f is the total fluid volume [L^3], μ is the dynamic viscosity [$(ML^{-1}T^{-2})$*T], A is the network cross-sectional area [L^2], and ΔP is the pressure difference [$ML^{-1}T^{-2}$] between the inflow and outflow boundaries.

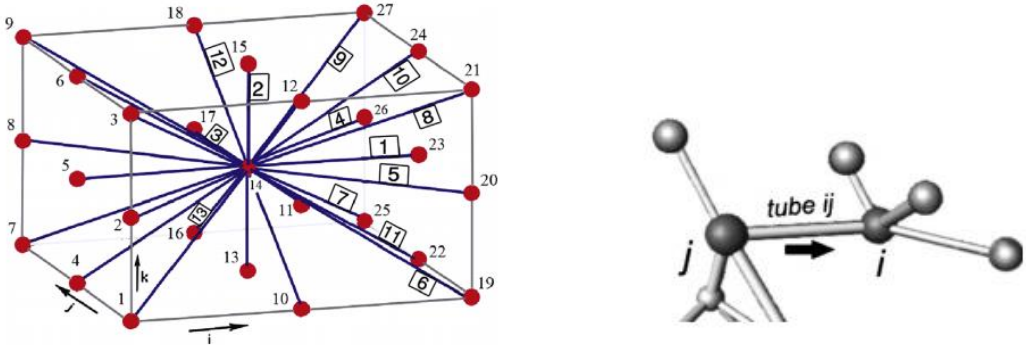

Figure 1
Left: Schematic of pore network consisting of 3 x 3 x 3 pore bodies, showing all 26 possible connections with pore body 14 (in the centre). Numbers inside squares denote throat directions and plain numbers are pore body numbers.
Right: Schematic of interconnected pore bodies and pore throats, showing flow direction from pore body j to pore body i through pore throat ij. From: Raoof et al. (2013)

2.2 PHREEQC

PHREEQC is a geochemical model capable of simulating a variety of geochemical reactions and transport processes, including speciation, batch reaction, 1-D transport and inverse modeling. PHREEQC evolved from the Fortran program PHREEQE [Parkhurst et al., 1980] which has been completely rewritten in C programming language and been regularly updated and extended since then. In this section a brief overview of the features relevant for this research are given, including speciation and reactive-transport calculations. More detailed and extensive information about PHREEQC can be found in [User's Guide to PHREEQC, version 2].

PHREEQC determines the speciation for a given solution, which may interact with solid and gas phases, by solving a set of functions derived from mole- and charge balance equations assuming the system is at equilibrium. Essentially the total element concentrations, which are constrained in the initial input, are redistributed among aqueous species assuming all reactions will reach instantaneous equilibrium. By default, the program assumes that there is 1 kg of water, as solvent for the solution, such that concentrations are expressed in molal units (moles per kg of water).

Incorporated in PHREEQC is an extensive database containing the necessary equilibrium reactions and constants which are required to formulate expressions for the number of moles of different types of species. All chemical reactions in PHREEQC are written in terms of "master species", which represent different elements and element valence states (i.e. Ca^{2+}, Fe^{2+}, Fe^{3+}). As such the amounts of species (moles) can be expressed in terms of these "master species", which vastly reduces the number of unknowns to be solved. The equations for the number of moles of species are then substituted in mole- and charge balance equations that are solved simultaneously using a modification of the Newton-Raphson method. This numerical method iteratively refines the values of the unknowns until the residuals are within a specified tolerance.

Aside from the equilibrium reactions there is also the possibility to include kinetic reactions in PHREEQC, for which the rate expressions can be incorporated by the user in the form of BASIC language statements. 1D transport processes such as advection, diffusion and dispersion are modelled in PHREEQC by solving the general advective-transport equation:

$$\frac{\partial C}{\partial t} = -v\frac{\partial C}{\partial x} + D_L\frac{\partial^2 C}{\partial x^2} - \frac{\partial q}{\partial t}, \qquad (6)$$

where C = concentration (mol/kgw), t = time (s), x = distance (m), v = velocity (m/s), D_L = dispersion coefficient (m^2/s) and q = concentration in solid phase (mol/kgw). On the right-hand side of the equation; the first term represents the advective transport, the second term represents the dispersive transport and the last term represent the change in concentration in the solid phase due to chemical reactions. PHREEQC considers a 1D column discretized into a number of cells (1 – n), for which the initial conditions, such as initial solution composition, can be defined individually for each cell. Transport through this column is calculated with the following split operator scheme, which is thought to minimize the numerical dispersion; advective transport – chemical reactions – dispersive transport – chemical reactions. First advection is calculated by simply shifting the solutions from one cell to the next, with the infilling solution always being solution number 0 (i.e. solution 0 to cell 1, solution in cell 1 to cell 2, and so on), then any cell-batch reactions are done (kinetic and/or equilibrium), followed by dispersion, which is essentially calculated as a mixing between neighbouring cells under the restriction that never more is mixed out than stays behind, and lastly cell-batch reactions are performed again. The most important user defined variables for these transport calculations are the number of cells, the number of shifts (how many times the solutions are shifted to the next cell), the time step (amount of time required to shift solution from one cell to the next) and the cell lengths. The velocity in each cell is determined by the cell length divided by the timestep and it is thus not possible to define the velocity explicitly.

3 Methods

3.1 Calcite dissolution kinetics

Over the past three decades the kinetics of calcite dissolution has been studied extensively in geochemical literature [e.g. Plummer et al. (1978); Chou et. al (1989); Sjöberg (1978); Arvidson et al. (2002)]. Despite some of the conjecture that still remains regarding the mechanisms involved and the absolute values of the rate under certain conditions, it is generally believed that the dissolution of calcite occurs via three parallel pathways. Here, we consider the three parallel reactions as proposed by Plummer et al. (1978) and Chou et al. (1989) (see Table 1).

Table 1:
Forward (dissolution) reactions with corresponding rate constants at 25°C and 50°C.
Rate constants at 50°C are derived assuming an Arrhenius type relation, using values at 25°C from Chou et al. (1989) and apparent activation energies from Plummer et al. (1979).

Forward (dissolution) reactions	*Rate constant (25°C)* [mol m^{-2} s^{-1}]	*Rate constant (50°C)* [mol m^{-2} s^{-1}]
$(R1)\quad CaCO_3(s) + H^+ \rightarrow Ca^{2+} + HCO_3^-$	$k_1 = 0.89$	$k_1 = 1.16$
$(R2)\quad CaCO_3(s) + H_2CO_3^* \rightarrow Ca^{2+} + 2HCO_3^-$	$k_2 = 5.01 \cdot 10^{-4}$	$k_2 = 1.85 \cdot 10^{-3}$
$(R3)\quad CaCO_3(s) \rightarrow Ca^{2+} + CO_3^{2-}$	$k_3 = 6.6 \cdot 10^{-7}$	$k_3 = 1.85 \cdot 10^{-6}$

Far from equilibrium and under low pH conditions, the first reaction is the dominant pathway. This reaction occurs at a much faster rate than the other two reactions. As the reaction progresses and pH increases, the second reaction will become dominant under high P_{CO2} conditions. Finally, when the reaction is near equilibrium, under high pH and low P_{CO2} conditions, the last reaction will become the dominant pathway. The forward rate of dissolution is thus determined by the sum of all three forward reactions and, following the principle of detailed balancing (i.e. microscopic reversibility), the backward rate is determined by the sum of all three backward reactions. Chou et al. (1989) have shown, however, that the backward rate of dissolution (precipitation) is only dependent on reaction (R3), leading to the following rate law for the dissolution of calcite:

$$Rate = k_1 \cdot \alpha_{H^+} + k_2 \cdot \alpha_{H_2CO_3^*} + k_3 - k_{-3}\alpha_{Ca^{2+}} \cdot \alpha_{CO_3^{2-}}, \qquad (7)$$

where $Rate$ is the net rate of dissolution [mol m^{-2} s^{-1}], k_1, k_2, k_3 are the forward rate constants of reactions (R1), (R2), and (R3) respectively, k_{-3} is the backward rate constant of reaction (R3), and α_x is the bulk activity of species x.

Furthermore, it is assumed here that reactions between aqueous species all attain instant equilibrium. With this assumption each individual reaction rate may be rewritten in terms of calcite saturation using the equilibrium constants given in Table 2. The overall rate of reaction can then simply be described in terms of distance from equilibrium:

$$Rate = \left(k_1 \cdot \alpha_{H^+} + k_2 \cdot \alpha_{H_2CO_3^*} + k_3\right) \cdot \left(1 - \frac{\alpha_{Ca^{2+}} \cdot \alpha_{CO_3^{2-}}}{K_{sp}}\right), \qquad (8)$$

where K_{sp} is the equilibrium constant of calcite.

Table 2:
Equilibrium dissociation reactions with corresponding equilibrium constants at 25.
[a] from Koutsoukos and Kontoyannis (1984)
[b] from Plummer and Busenberg (1982)

Equilibrium reactions	*Equilibrium constant (25°C)*
$(R4) \quad HCO_3^- \leftrightarrow H^+ + CO_3^{2-}$	$K_1 = 4.446\text{e}-7$ [a]
$(R5) \quad H_2CO_3^* \leftrightarrow H^+ + HCO_3^-$	$K_2 = 4.688\text{e}-11$ [a]
$(R6) \quad CaCO_3(s) \leftrightarrow Ca^{2+} + CO_3^{2-}$	$K_{sp} = 3.31\text{e}-9$ [b]

Note that by using bulk activities in the above reactions it is essentially assumed that the dissolution rate is reaction-limited and thus not inhibited by the transport of species from the bulk solution to the reactive surface. This is of course the case for well-mixed systems where there is a uniform concentration, which for single pores in calcite occurs under flow conditions slower than 0.001 cm/s or faster than 1000 cm/s [Li et al., 2008]. However, in reality, these flow conditions cannot always be guaranteed during CO_2 injection/storage and transport limitations should thus be accounted for to ensure the rate of reaction is not overestimated. This is not an issue for models where pore spaces are discretized into cells (e.g. Lattice Boltzmann) because transport effects are already incorporated into the concentration calculations for each cell. However, in pore-network models, where concentration gradients within pores are not considered and thus only average concentrations within the pore-spaces are known, transport limitations will need to be accounted for in some other way.

3.2 Network generation

The pore-networks implemented in this model are generated in PoreFlow for a specified pore-body radius distribution and average coordination number (see section 3.4). As previously stated, PoreFlow allows for a maximum coordination number of 26, which means that a given pore-body may be connected to a maximum of 26 neighbouring pore-bodies. To achieve a specified average coordination number PoreFlow employs an elimination procedure to rule out some of the connections. The details of this elimination procedure are discussed in more detail in Raoof and Hassanizadeh (2009).

For a given pore-body radius distribution PoreFlow calculates the corresponding pore-throat radii by using the BACON bond method from Acharya et al. (2004). They use two simple power-functions to construct a biconical shaped pore-throat connecting two spherical pore bodies (see Figure 2). The radius of the narrowest section of the pore-throat connecting pore bodies i and j, located at the point of intersection between the two power functions (ξ_t), is determined by:

$$r(\xi_t) = T_i T_j (T_i^{\frac{1}{n}} + T_j^{\frac{1}{n}})^{-n}, \quad n > 0 \tag{9}$$

Where $r(\xi)$ is the dimensionless bond-size function along the central axis (ξ) of the pore-throat, n is the curvature parameter that determines the longitudinal shape of the function and T_i and T_j are the values of $r(\xi)$ at the corresponding pore body centres and are calculated by:

$$T_i = \frac{\tilde{R}_i \sin(\frac{\pi}{\zeta})}{[1-\tilde{R}_i \cos(\frac{\pi}{\zeta})]^n}, \quad n > 0 \tag{10}$$

$$T_j = \frac{\tilde{R}_j \sin(\frac{\pi}{\zeta})}{[1-\tilde{R}_j \cos(\frac{\pi}{\zeta})]^n}, \quad n > 0 \tag{11}$$

$\tilde{R}_i$ and $\tilde{R}_j$ represent the dimensionless pore body sizes and $\frac{\pi}{\zeta}$ is the angle BAF under bisector AF for pore body i and the angle GBA under the bisector BG for pore body j.

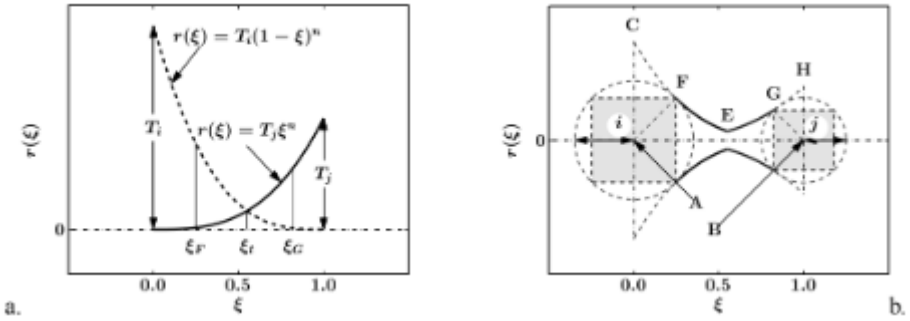

Figure 2
Construction of the BACON bond, from [Acharya et al., 2004]. a) Showing the power law functions describing the radius as a function of ξ (scaled distance between pore-bodies). The centre of pore body i is located at ξ = 0 and the centre of pore body j is located at ξ = 1. The pore-throat inlet and outlet are located at ξ_F and ξ_G respectively, and the ξ_t is the point of intersection and the narrowest section of the pore-throat. b) Showing the outline of the pore-throat walls (thick lines) connecting pore body i and j.

Instead of assuming biconical shaped pore-throats this model assumes cylindrical pore-throats that have a fixed radius along the entire length of the pore-throat, equal to the narrowest section of the biconical pore-throat in the BACON bond method. Here, the radius of pore-throats is calculated using equation (9) with a curvature parameter of *0.3*. This simplification of pore-throat geometry could, however, underestimate the amount of friction on the flow at the inlet and outlet of the pore-throat. To compensate for this, PoreFlow enhances the length of a given pore-throat depending on the pore-body surface areas of the connected pore bodies and their respective coordination numbers. The pore-throat length between two adjacent pore bodies is initially determined by the lattice distance minus the respective pore-body radii, after which a fraction of the surface area of both connecting pore bodies is added to this length. This fraction is equal to the total surface area of the pore body divided by the number of pore-throats connected to the pore body (i.e. coordination number).

3.3 Modeling approach

The previously introduced PHREEQC and PoreFlow models are coupled to develop an up scaled pore-network model with which to simulate reactive transport for CO_2 storage applications. The basic concept of the coupled model is visualized in Figure 3. The model discretizes a 3D pore network, generated in PoreFlow, into a series of cells over which PHREEQC is then able to perform 1D reactive transport calculations. For each of these cells PoreFlow determines the specific reactive surface area needed for the reaction calculations and outputs these to PHREEQC. PHREEQC then performs a reactive transport step and outputs the calculated change in calcite back to PoreFlow. PoreFlow distributes the volume of dissolved/precipitated calcite, generated from PHREEQC, over the pore spaces and recalculates the specific surface area required for the subsequent reactive transport step. PHREEQC and PoreFlow are thus run consecutively for each time step whilst information is fed back and forth between the two models.

This coupled model is therefore able to perform simple 1D reactive transport calculations whilst still taking into account the effect of pore-structure. Instead of having to consider each individual pore-body and pore-throat, of which a vast amount exist within a pore-structure, transport and reaction calculations are only necessary for a small number of cells, which reduces the computational run-time considerably.

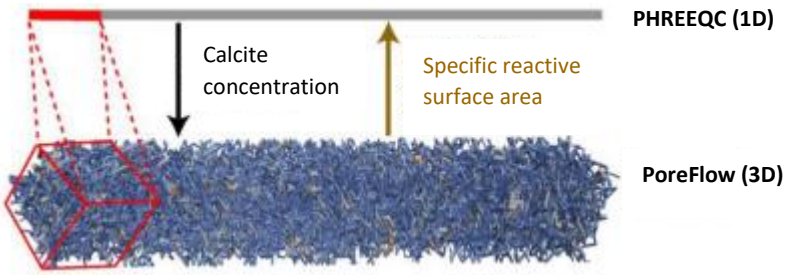

Figure 3
Coupling between PHREEQC and PoreFlow, adapted from [Ameri et al., 2017].

Several assumptions are made regarding the distribution of calcite over the network and the resulting changes in pore-structure. For simplicity it is assumed that dissolution occurs only within pore-throats and solely affects the pore-throat radius. Pore-body sizes and pore-throat lengths thus remain fixed throughout the reactive transport simulations. As such the surface area that is outputted from PoreFlow to PHREEQC only includes the pore-throat surface area. Furthermore, the amount of dissolved/precipitated calcite in each pore-throat is assumed here to be related to their relative residence times, defined as the volume over the discharge:

$$T_{res,ij} = \frac{V_{ij}}{Q_{ij}} = \frac{\pi \cdot R_{ij}^2 \cdot L_{ij}}{Q_{ij}}, \quad (12)$$

Where $T_{res,ij}$ is the residence time for a given pore-throat with radius R_{ij} and length L_{ij}.
By arguing that a lower-residence time allows for more reactive solution to pass through a given pore-throat and thus for more reactions to occur, it is assumed here that pore-throats with lower residence times dissolve more than pore-throats with higher residence times. As such a larger fraction of the total change in calcite will be attributed to pore-throats with lower residence times. The change in volume due to dissolution/precipitation for a given pore-throat, $dV_{cal,ij}$, is calculated with the following equation:

$$dV_{cal,ij} = \frac{dV_{cal,total} \cdot \frac{1}{T_{res,ij}}}{\sum \frac{1}{T_{res}}}, \quad (13)$$

where $dV_{cal,total}$ is the total volume change for the whole cell, $\frac{1}{T_{res,ij}}$ is the inverse residence time for that pore-throat and $\sum \frac{1}{T_{res}}$ is the sum of all inverse residence times of all pore-throats belonging to the same cell. Considering that the volume of a given pore-throat after dissolution should equal the original volume before dissolution plus the volume of dissolved/precipitated calcite the following equation applies for cylindrical pore-throats:

$$\pi \cdot R_{ij,new}^2 \cdot L_{ij} = \pi \cdot R_{ij,old}^2 \cdot L_{ij} + dV_{cal,ij}, \quad (14)$$

By rearranging the above equation, the new pore-throat radius is calculated as follows:

$$R_{ij,new} = \sqrt{R_{ij}^2 + \frac{dV_{cal,ij}}{\pi \cdot L_{ij}}}. \quad (15)$$

The new pore-throat radius may also be described as the sum of the old pore-throat radius and the change in pore-throat radius, and as such the following equation for the change in pore-throat radius applies:

$$dR = \sqrt{R_{ij}^2 + \frac{dV_{cal,ij}}{\pi \cdot L_{ij}}} - R_{ij} \quad (16)$$

If the pore-throat radius R_{ij} is very large, $\frac{dV_{cal,ij}}{\pi \cdot L_{ij}}$ becomes negligible and the radius thus does not change much. However, for a small pore throat radius the second term in the square root has a much bigger affect and so the pore-throat increases more. So, the relative change in pore-throat radius due to dissolution/precipitation reactions increases for smaller initial pore-throat radii.

A schematic flowchart of the coupled modeling procedure is given in Figure 4 and is explained in more detail below. After generating the initial network, PoreFlow is run with a zero change in calcite to determine the total initial reactive surface area for each cell which is then written to *PHREEQC_CELL_INFO.TXT*. Note that since dissolution is assumed to only occur within pore-throats, this surface area thus also only includes pore-throat surface areas. PHREEQC and PoreFlow then run consecutively in a loop over a specified number of time steps. In PHREEQC all cells are initially filled with a solution of water in equilibrium with calcite and are all given the same initial porosity equal to the total network porosity determined in PoreFlow. All cells are given an initial amount of calcite available for reaction (in moles), set to 10% of the initial solid volume of the pore-network cell to simulate a sandstone with a 10% volume fraction of calcite. The injecting solution is composed of water in equilibrium with CO_2 at a partial pressure of 10MPa to simulate the high-pressure conditions during CO_2 storage. With these initial conditions and the initial specific reactive surface area from PoreFlow, PHREEQC performs a 1D reactive transport shift and outputs the new solution composition and kinetic reactant data to a dump file. This file is written in a format which enables it to be incorporated directly as input for the subsequent transport step. PHREEQC also outputs the amount and change in calcite per cell to an output file called *delCalcite.txt* which will be used as input for PoreFlow. After PHREEQC has completed the reactive transport step, PoreFlow is run with the *delCalcite.txt* as input to recalculate the pore-throat radii (see Equation 15) and corresponding new pore-throat areas. *PHREEQC_CELL_INFO.TXT* is rewritten with the new total specific surface area per cell, such that it may be implemented in PHREEQC in the next loop. In this way PHREEQC and PoreFlow are run consecutively in a loop for a specified number of time steps, updating the various input and output files after each run.

It is important to note that whilst PoreFlow and PHREEQC use the same cell-sizes they do not assume the same fluid volume per cell, which requires the output exchanged between PHREEQC and PoreFlow to be scaled. PHREEQC by default assumes 1 liter of water for the batch reaction calculations regardless of the fluid volumes in the pore-network. As such the total surface area per cell calculated in PoreFlow is scaled up to a specific surface area per liter and the amount of calcite calculated in PHREEQC is conversely scaled down from a liter to the pore-network fluid volume for the corresponding cell in PoreFlow. The full model code including the batch executable and PoreFlow and PHREEQC input files can be found in the Appendix.

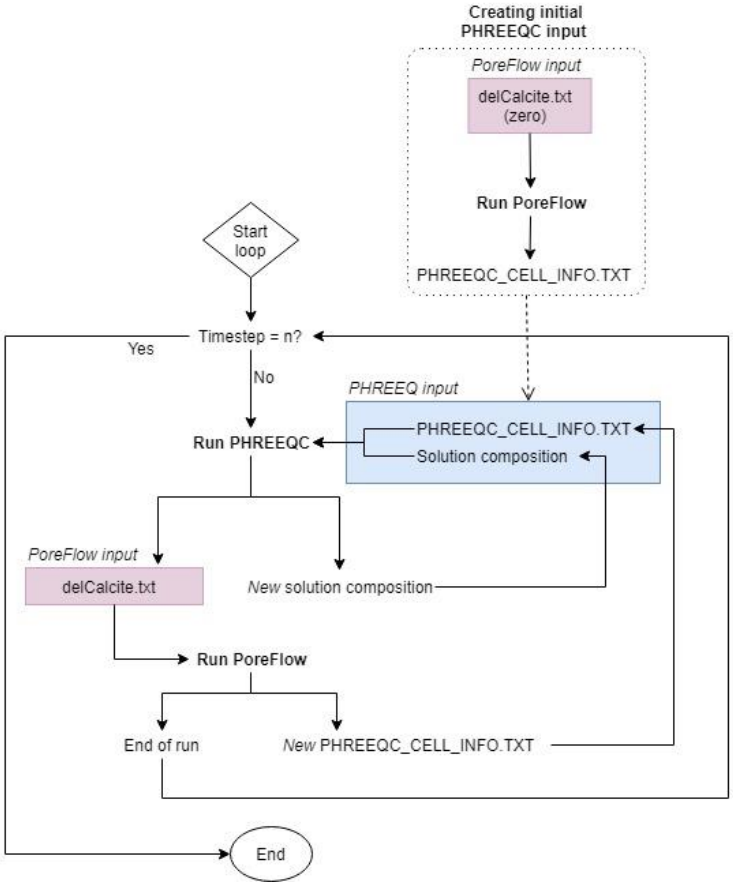

Figure 4
Flowchart of model procedure.

3.4 Model configuration

To investigate the effect of the pore-network structure on the dissolution of calcite 18 different initial pore-networks are generated, varying in average coordination number and pore-size distribution. These networks are generated from six lognormal pore-size distributions with mean values of 200, 300 and 400 um and standard deviations of 30 and 86 um (see Fig. 5), and three different average coordination numbers (3, 4 and 5). These mean pore-sizes are chosen to simulate sandstone, which are generally found to have relatively large pore sizes[1].

All networks have a total network length of ~95 mm and are discretized into 20 cells with lengths of ~4.8 mm and volumes of ~1540 mm^3. Networks with a mean pore-size of 200, 300 and 400 um are given an initial network porosity of 0.15, 0.20 and 0.25, respectively. These porosities are achieved by adjusting the number of nodes (pore bodies) and the lattice distance (distance between pore body centres) for each network. For instance, networks with a larger mean pore-size and/or larger average coordination number will automatically have a larger porosity, however by increasing the lattice distance and/or decreasing the number of nodes the porosity can be lowered. The ratio of number of nodes in each direction is kept at 5:1:1 (Ni:Nj:Nk) for all networks. The initial network properties are summarized in Table 3. The different networks are referred to by a code starting with a capital letter

[1] There may be a minor fault in that the mean pore-size values used here actually resemble sandstone *grainsizes* rather than pore sizes, and are thus around an order magnitude larger than what is typically found in literature [Philip Nelson, 2009][Dong and Blunt 2009]. The networks generated here thus represent (unrealistically) coarse sandstone.

to identify the mean pore-body radius of the network: A, B and C are networks with mean pore-body radius of 200, 300 and 400 um respectively. Next the corresponding standard deviation of the pore-body radius distribution is denoted by L for low standard deviation (30 um) and H for high standard deviation (86/87 um). And lastly, the coordination number (3, 4 or 5) is given. As an example, AL-3 is the network generated from a mean pore-radius of 200 um with standard deviation 30 um and coordination number 3.

For the pore-structure analysis all networks are run for 500 pore volumes with the following input parameters in PHREEQC. Time-steps in PHREEQC (the duration of a single shift) are set to 0.025 seconds, corresponding to a velocity of ~193 mm/s. This high velocity is chosen to ensure that dissolution occurs uniformly along the length of the column (see section 4) [Golfier et al. 2001], making for better analysis of pore-structure parameters. Dispersivities are set to 10% of the cell length. Networks A, B and C are given 15, 11 and 8 moles of calcite per cell (concentrations per litre!) respectively, which amounts to about 10% of the initial solid volume per cell. High temperature and pressure conditions are simulated in PHREEQC by using a CO_2 partial pressure of 10MPa and reaction constants valid at a temperature of 50°C (see Table 1 and 2). This temperature is also accounted for in the viscosity used by PoreFlow and is set to a value of 0.0005 Pa·s [Engineering ToolBox, 2004]. Lastly, since porosity changes are likely minimal after a single shift (time-step is very short) it is not necessary to update the pore-network after each individual shift. To reduce the computational expense of the model PHREEQC is run consecutively for 250 shifts (corresponding to 12.5 pore volumes and 6.25 seconds) before coupling with PoreFlow.

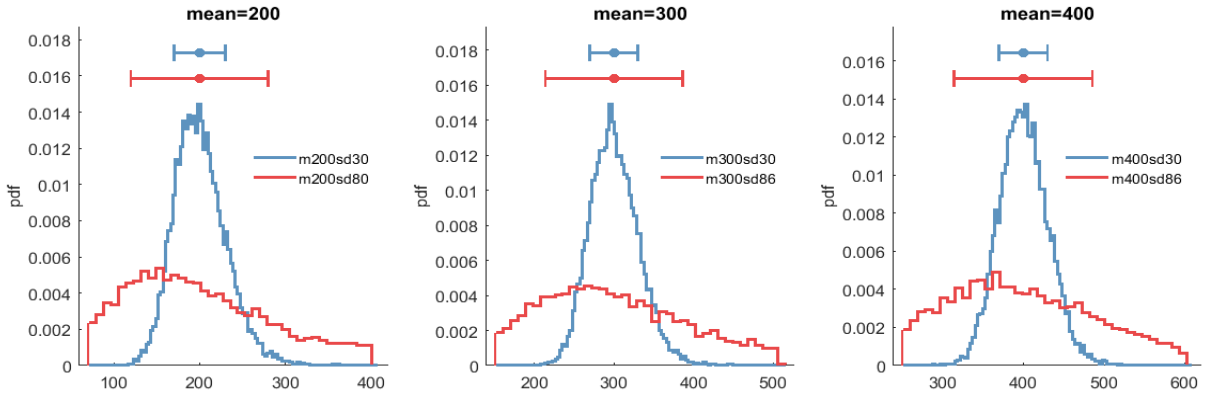

Figure 5
Probability density distributions of pore-radius with mean of 200, 300 and 400 um and standard deviation of 30 (blue) and 86 um (red), used for initial pore size generation.

Table 3

Initial network properties. Networks are grouped according to mean pore-body radius and coordination number. Ni, Nj and Nk = number of nodes in each dimension, Ncont = lattice distance, Net. Length = network length, Ntube = number of pore-throats, Nnode = number of pore bodies, Vtot = total volume of network, Vf = total fluid volume of network (volume of pore bodies and throats), A_pipe = total surface area of pore-throats, A_specific = specific surface area for the whole network (Piper area/Vf).

Network	*Mean [um]*	*Stdev [um]*	*Coord. nr.*	*Ni*	*Nj*	*Nk*	*Ncont [um]*	*Net. length [mm]*	*Cell length [mm]*	*Ntube*	*Nnode*	*Porosity*	*Vtot [mm3]*	*Vf [mm3]*	*A_pipe [mm2]*	*A_specific [m2/L]*
AL-3	200	30	3	113	22	22	850	95,20	4,80	65315	40120	0,15	30333	4615,17	5,35E+04	11,59
AH-3	200	87	3	113	22	22	850	95,20	4,80	65315	40120	0,16	30333	4956,11	4,92E+04	9,92
AL-4	200	30	4	96	19	19	1002	95,19	4,81	60233	30354	0,15	30965	4579,10	5,88E+04	12,84
AH-4	200	87	4	96	19	19	1002	95,19	4,81	60233	30354	0,15	30965	4690,89	5,35E+04	11,41
AL-5	200	30	5	86	17	17	1120	95,20	4,82	55077	23301	0,14	30571	4234,08	5,72E+04	13,52
AH-5	200	87	5	86	17	17	1120	95,20	4,82	55077	23301	0,14	30571	4161,02	5,10E+04	12,26
BL-3	300	30	3	80	16	16	1200	94,80	4,80	23607	14729	0,20	30715	6033,96	4,69E+04	7,78
BH-3	300	86	3	80	16	16	1200	94,80	4,80	23607	14729	0,20	30715	6169,72	5,96E+04	9,67
BL-4	300	30	4	70	14	14	1380	95,22	4,83	23037	11818	0,21	30646	6477,95	5,54E+04	8,55
BH-4	300	86	4	70	14	14	1380	95,22	4,83	23037	11818	0,21	30646	6520,24	5,38E+04	8,25
BL-5	300	30	5	65	13	13	1488	95,23	4,84	23695	10196	0,20	30363	6081,71	5,32E+04	8,75
BH-5	300	86	5	65	13	13	1488	95,23	4,84	23695	10196	0,20	30363	5984,85	5,07E+04	8,47
CL-3	400	30	3	80	16	16	1412	94,60	4,80	14882	9396	0,26	31876	8248,55	4,50E+04	5,45
CH-3	400	86	3	80	16	16	1412	94,60	4,80	14882	9396	0,26	31876	8340,36	4,41E+04	5,28
CL-4	400	30	4	70	14	14	1660	94,62	4,81	13665	7092	0,26	31549	8216,62	4,96E+04	6,03
CH-4	400	86	4	70	14	14	1660	94,62	4,81	13665	7092	0,26	31549	8150,37	4,83E+04	5,93
CL-5	400	30	5	65	13	13	1795	95,14	4,85	13797	6061	0,25	30653	7575,58	4,68E+04	6,18
CH-5	400	86	5	65	13	13	1795	95,14	4,85	13797	6061	0,24	30653	7398,10	4,51E+04	6,09

4 General model behaviour and velocity

First, an initial analysis is performed to investigate the general model behaviour for different flow velocities. Network AL-5 is run using time-steps of 1, 0.5, 0.1, 0.05 and 0.025 seconds, corresponding to velocities of 4.82, 9.63, 48.16, 96.32 and 192.64 mm/s respectively. To facilitate run time PoreFlow and PHREEQC are coupled every 20 pore volumes, meaning PoreFlow updates the pore-network every 400 shifts. Such a large coupling interval could potentially cause significant inaccuracies, especially when using relatively slow velocities seeing as a larger reaction time results in larger changes in porosity. However, for the slowest velocity (i.e. 4.82 mm/s) the differences in results found using an interval of 20 pore volumes and a more frequent interval of 1 pore volume are still relatively small (see Appendix). After 60 pore volumes the maximum difference in porosity between the two coupling intervals is 0.02 and on average only 0.002. Also, the difference in calcite concentration is minimal with a maximum difference of only 0.11 mol. Considering these inaccuracies are even smaller for the faster velocities it is thus assumed that a coupling interval of 20 pore volumes is still sufficient to ensure an accurate analysis of the effect of velocity on the dissolution behaviour. Lastly, network CL-5 is run for a single pore volume using 8 mmol of initial calcite per cell and time-steps of 60 seconds (v = 0.08 mm/s).

The calcite and pH distribution after 0.5 pore volume, for a velocity of 0.08 mm/s (times-step = 60 seconds), are presented in Figure 6. The calcite distribution shows that after 0.5 pore volume (10 minutes) all the calcite in cells 1 – 9 has dissolved, whilst no net-dissolution of calcite has occurred in cells 15 – 20. The pH distribution shows a distinct three-step increase in pH toward the outlet where the first step, close to the inlet, coincides with the equilibrium pH for a solution in equilibrium with CO_2 (equal to injection solution pH with a value of 3.2), the second step is less pronounced but roughly coincides with the equilibrium pH for a solution in equilibrium with CO_2 and calcite, and finally the third step coincides with the equilibrium pH for a solution in equilibrium with calcite (equal to initial solution pH with a value of 9.4). It is interesting to see that these steps in pH do not coincide directly with the calcite distribution. For example, even though cells 6 – 9 are depleted in calcite their pH values are higher than the injection solution pH, which shows that these cells have not yet been flushed out completely. Similarly, at the outlet the pH in cells 15 and 16 has decreased even though their calcite concentrations have not. This observation can be explained by dispersion, simulated in PHREEQC as a partial mixing of neighbouring cells, which makes the speciation in a given cell not only dependent on its incoming solution but rather on all neighbouring cells.

In Figure 7 the calcite and pH distributions for a range of different velocities are shown. The calcite distribution plot (left) shows that for high velocities the dissolution occurs uniformly over the column, whereas for low velocities the dissolution is predominately occurring at the inlet (i.e., face dissolution). This is to be expected considering the reaction time scale is larger than the flow time scale (i.e., the solution reaches deeper into the sample before it dissolved much calcite and is buffered). Conversely, slow velocities provide longer reaction times causing more CO_2 to be consumed at the inlet leaving less to react in the subsequent cells. This is confirmed by the pH distribution that shows lower pH values at the outlet for faster velocities. At the inlet, however, the pH values for the two slowest velocities are lower because the calcite is running out in the first cells which causes the pH to drop toward a new equilibrium. Furthermore, the pH in all cells has dropped below the initial equilibrium (upper step in Figure 6) because the column has already been flushed through completely (60 times) such that all cells contain some degree of CO_2. On the other hand, in Figure 6 the initial pH front is still visible because it has not reached a full pore volume yet.

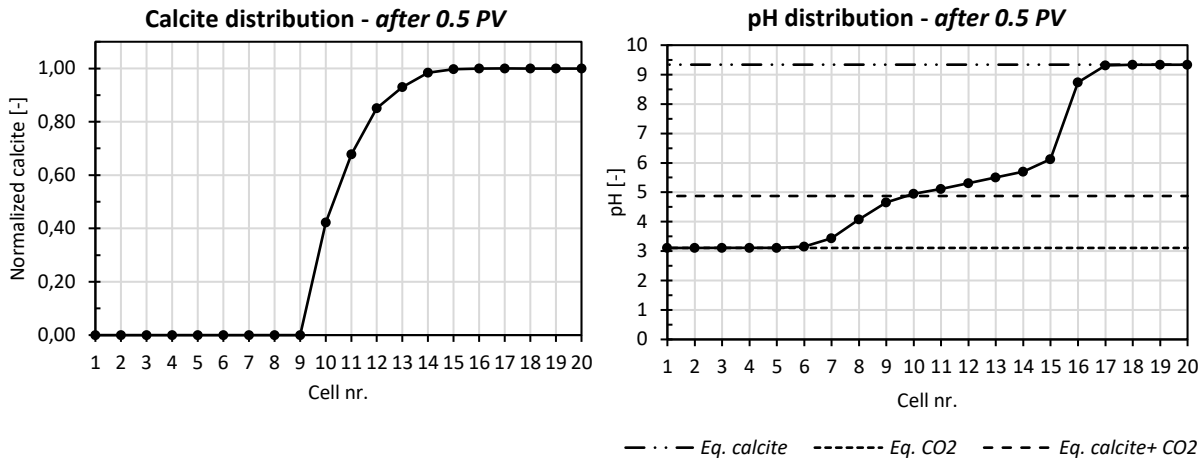

Figure 6
Left: calcite distribution in network CL-5 after 0.5 pore volumes, run with velocity of 0.08 mm/s (time-step = 60 seconds). Calcite is normalized over the initial calcite per cell = 8 mol. Right: corresponding pH distribution and three equilibrium pH values (dash lines). Eq. calcite (initial solution) = 9.34, eq. CO2 (injection solution) = 3.11 and eq. calcite + CO2 = 4.84.

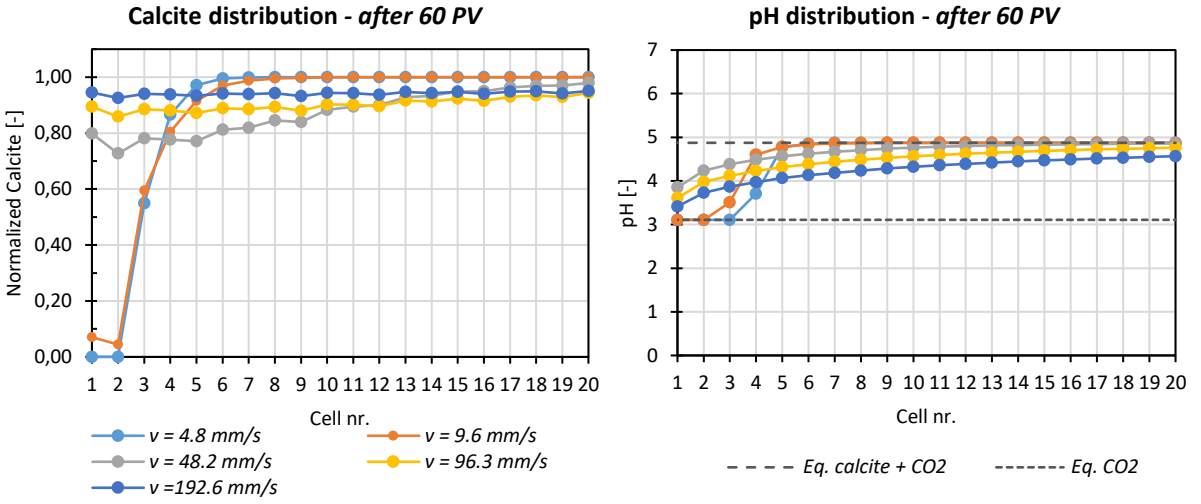

Figure 7
Left: calcite distribution in network AL-5, after 60 pore volumes. Calcite is normalized over the initial calcite per cell = 15 mol. Right: corresponding pH distribution and three equilibrium pH values (dash lines).

In Figure 8a the amount of dissolved calcite is plotted against pore volumes for the different velocities. For all simulations the increase in dissolved calcite is seen to become linear after about 1 pore volume, which points to a steady-state dissolution behaviour.

Figure 8b shows the porosity-permeability curves for the different velocity simulations, where each data point represents 20 pore volumes. Most notable is the shape of the porosity-permeability curves which differs from the usual convex shape (starting out relatively flat and becoming steeper as porosity increases) where the change in permeability becomes progressively larger as porosity increases. Here, the change in permeability is seen to first decrease and then increase with increasing porosity (two inflection points as opposed to one). A similar curve is found when plotting porosity against mean pipe radius. This initial decrease in the rate of increase in permeability may be explained by the fact that the network consists of pore-throats of varying sizes which have varying rates of radius increase. For a given volume of dissolved calcite the resulting pore-throat radius

increase is larger for small pores than for large pores (see Equation 16) because large pores need to distribute the amount of dissolved calcite over a much larger surface area. Thus as dissolution occurs, small pores could cause the average radius to initially increase significantly but as they become larger the increase in radius will become progressively smaller. Since pore-throat radius is directly related to permeability this may explain why the permeability change is initially seen to decrease. Furthermore, it can be seen from Figure 8b that the porosity increase is greater for slower velocities. For example, after 100 pore volumes the fastest velocity has increased to 0.156 whereas the slowest has only reached a porosity of 0.146 after the same number of pore volumes. This is confirmed by the dissolution plot in Figure 8b, where steeper increases in total amount of dissolved calcite are seen for the slower velocities. Contrary to porosity, the permeability increase after 100 pore volumes is greatest for the intermediate velocities and slowest for the two extremes. Permeability is thus not only influenced by the relative amount of dissolution but also by the distribution of porosity throughout the column. In the case of extremely fast flow there is so little dissolution that the permeability is hardly affected, and in the case of extremely slow flow dissolution is only occurring at the inlet leaving most of the network unaffected. Furthermore, the permeability at a given porosity is lowest for the two slowest velocities which can again be explained by the lack of uniform dissolution which inhibits permeability. At a porosity of 0.145 the three faster velocities give the same permeability value (graphs intersect). However, even though the velocities all reach the same value the amount of pore volumes it takes to reach this point does differ. With a velocity of 192.64 mm/s it takes 80 pore volumes to increase the permeability by ~9 % while it only takes 40 pore volume with a velocity of 48.16 mm/s.

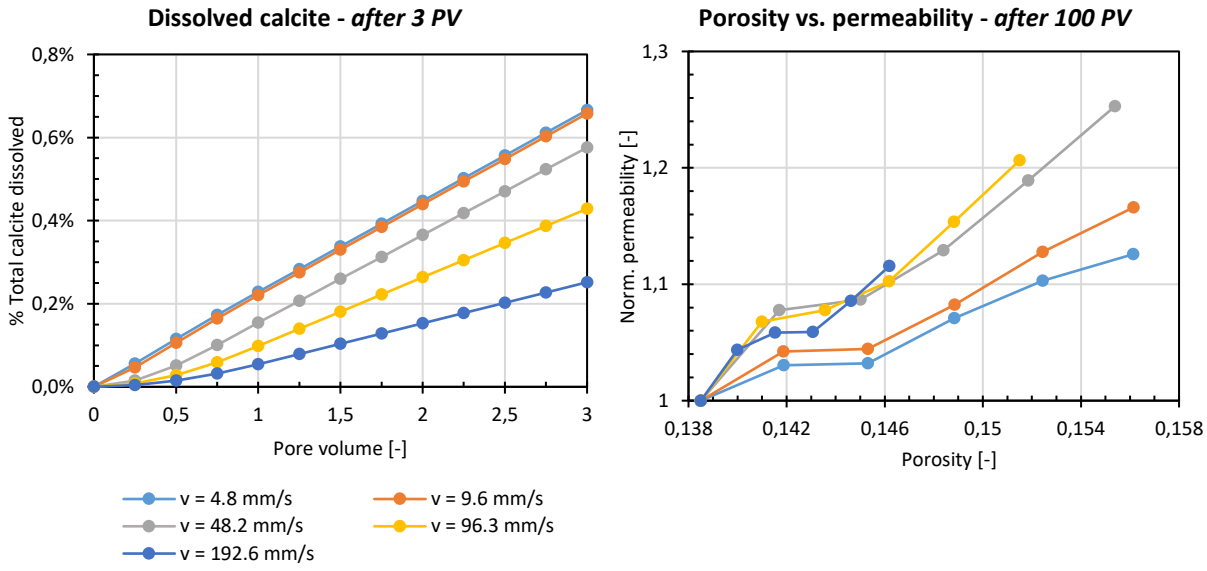

Figure 8
Left: total dissolved calcite over 3 pore volumes using network AL-5. Dissolved calcite is normalized over the total initial calcite, 20 x 15 moles = 300 moles. Right: corresponding porosity- permeability evolution during 100 pore volumes (in steps of 20 pore volumes). Permeability is normalized with the initial network permeability (= 5.31E-11).

5 Results

Using a velocity of 192.64 mm/s (time-step of 0.025 seconds) the following result were obtained for the different networks. Results for network AL-4 could not be obtained due to an error in PoreFlow which, unfortunately, could not be resolved in time!

Figure 9 shows the porosity increase over 500 pore volumes for the different networks and the corresponding rate of increase is given in Table 4. These rates can be compared to investigate the relative effects of mean pore-size, standard deviation and coordination number. Firstly, the results indicate that the porosity increases faster for a lower mean pore-size. In comparing differences in standard deviation the results show that networks with a low standard deviation increase in porosity faster than networks with a high standard deviation. And lastly, a coordination number of 4 seems to give the highest rate of porosity increase.

Figure 10 shows the calcite distribution over the network after 500 pore volumes and it can be seen that overall distribution is rather uniform for the different networks (as expected for the high velocity used). The individual calcite concentrations per cell do, however, show variations and seem to be dependent on the initial mean pore-body radius.

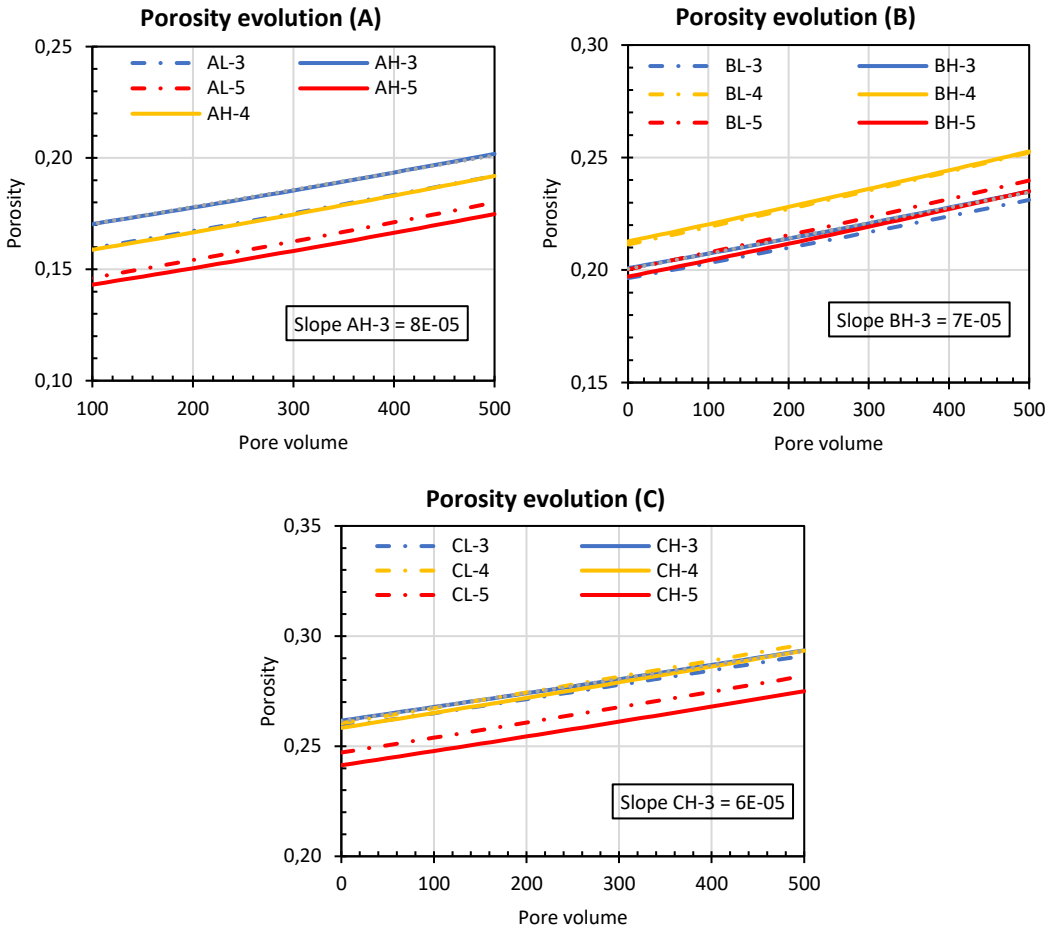

Figure 9
Porosity evolution for different networks A, B and C (mean pore-body radius 200, 300 and 400µm respectively). Pore networks are further identified by a letter L or H to denote a low or high standard deviation, respectively, and a number to indicate the average coordination number.

Table 4
Rate of porosity increase [1/pore volume].

AL-3	7.96E-05	***BL-3***	6.95E-05	***CL-3***	6.48E-05
AH-3	7.71E-05	***BH-3***	6.81E-05	***CH-3***	6.38E-05
AL-4	-	***BL-4***	8.17E-05	***CL-4***	7.17E-05
AH-4	8.10E-05	***BH-4***	8.00E-05	***CH-4***	7.01E-05
AL-5	8.31E-05	***BL-5***	7.90E-05	***CL-5***	6.96E-05
AH-5	7.75E-05	***BH-5***	7.59E-05	***CH-5***	6.73E-05

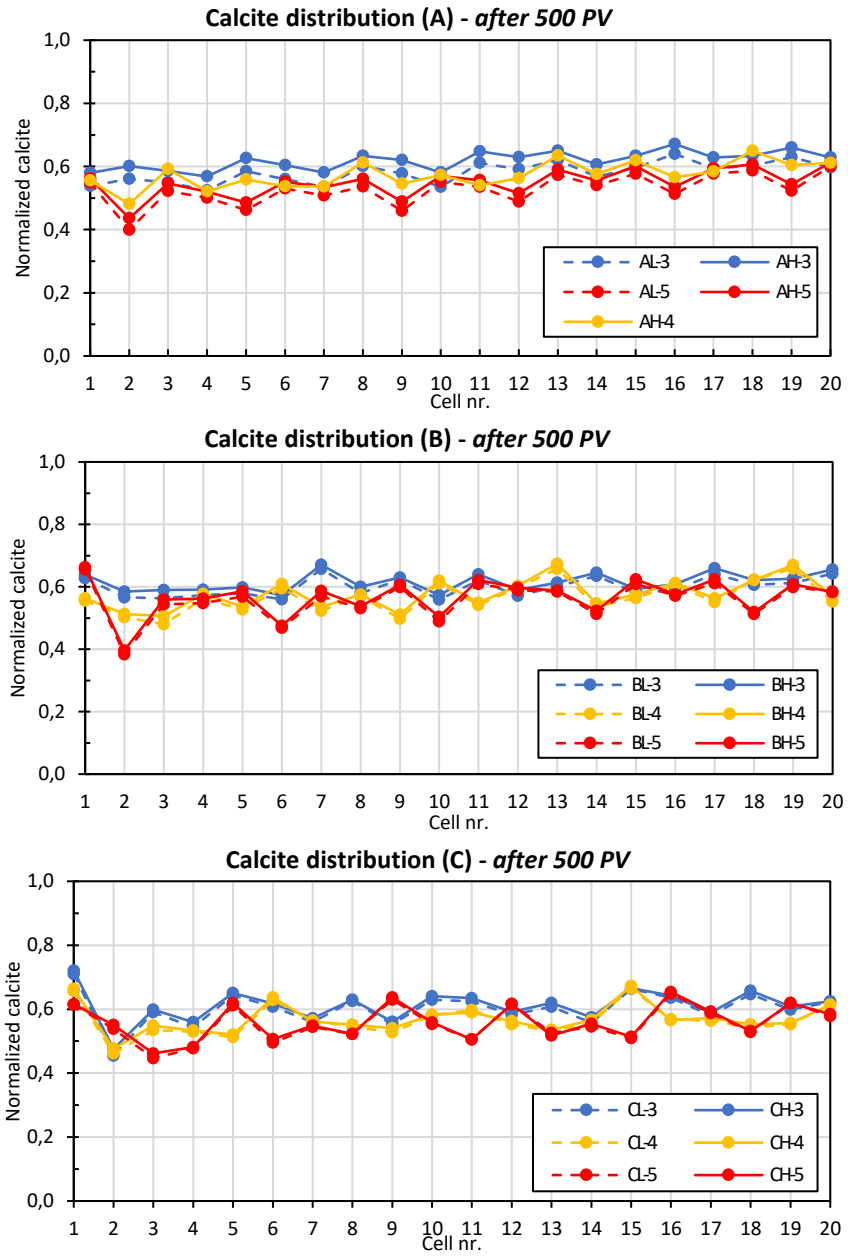

Figure 10
Calcite distribution after 500 pore volumes for all the networks A (top), B (middle) and C (bottom). Solid lines are networks with low standard deviation and dashed lines are network with a high standard deviation. Colours red, orange and blue denote coordination numbers 3, 4 and 5 respectively. Calcite is normalized over the initial calcite.

The following results show the relative effect of the initial pore-structure on the pore size distribution. Since dissolution is assumed to occur only within pore-throats, only the pore-throat distribution is affected. Thus, pore-body distribution and pore-throat length distributions remain unchanged.

For all networks the mean pore-throat radius is seen to increase linearly over time ($R^2 = 1$) with the slight exception of networks AL-* and AH-* which are a little less linear, shown in Figure 11. The complete set of figures for all networks can be found in the Appendix. The rate of increase in mean pore-throat radius is given in Table 5 and is on average around 0.04 um per pore volume for all networks. Within network B and C the differences are minimal whereas differences within network A are larger, showing faster increase in mean pore-throat radius for networks with a large initial standard deviation. On average, networks with a larger initial mean pore-size show a slightly larger increase in mean pore-throat radius.

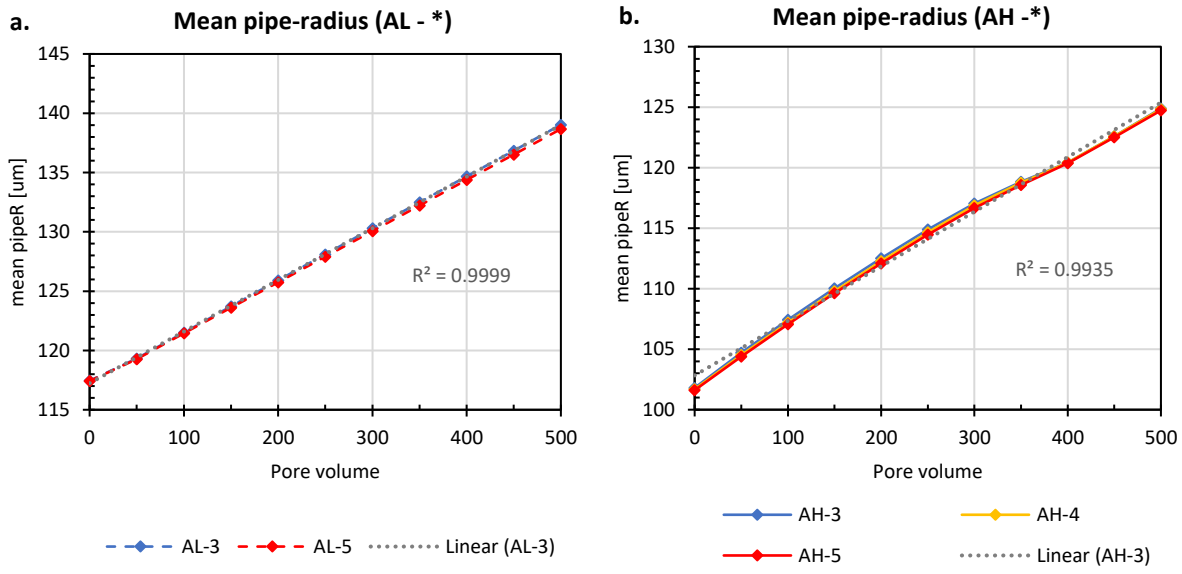

Figure 11
Mean pore-throat radius evolution over 500 pore volumes (in steps of 50 pore volumes) for networks AL-* (left) and networks AH-* (right). Trend lines for aL-3 and aH-3, with their corresponding R^2, are plotted as well. Data for AL-4 is missing!

Table 5
Rate of mean pore-throat increase in um/pore volume.

AL-3	3.75E-02	***BL-3***	4.47E-02	***CL-3***	4.60E-02
AH-3	5.80E-02	***BH-3***	4.40E-02	***CH-3***	4.71E-02
AL-4	-	***BL-4***	4.41E-02	***CL-4***	4.54E-02
AH-4	5.63E-02	***BH-4***	4.48E-02	***CH-4***	4.65E-02
AL-5	3.71E-02	***BL-5***	4.45E-02	***CL-5***	4.61E-02
AH-5	5.56E-02	***BH-5***	4.40E-02	***CH-5***	4.68E-02

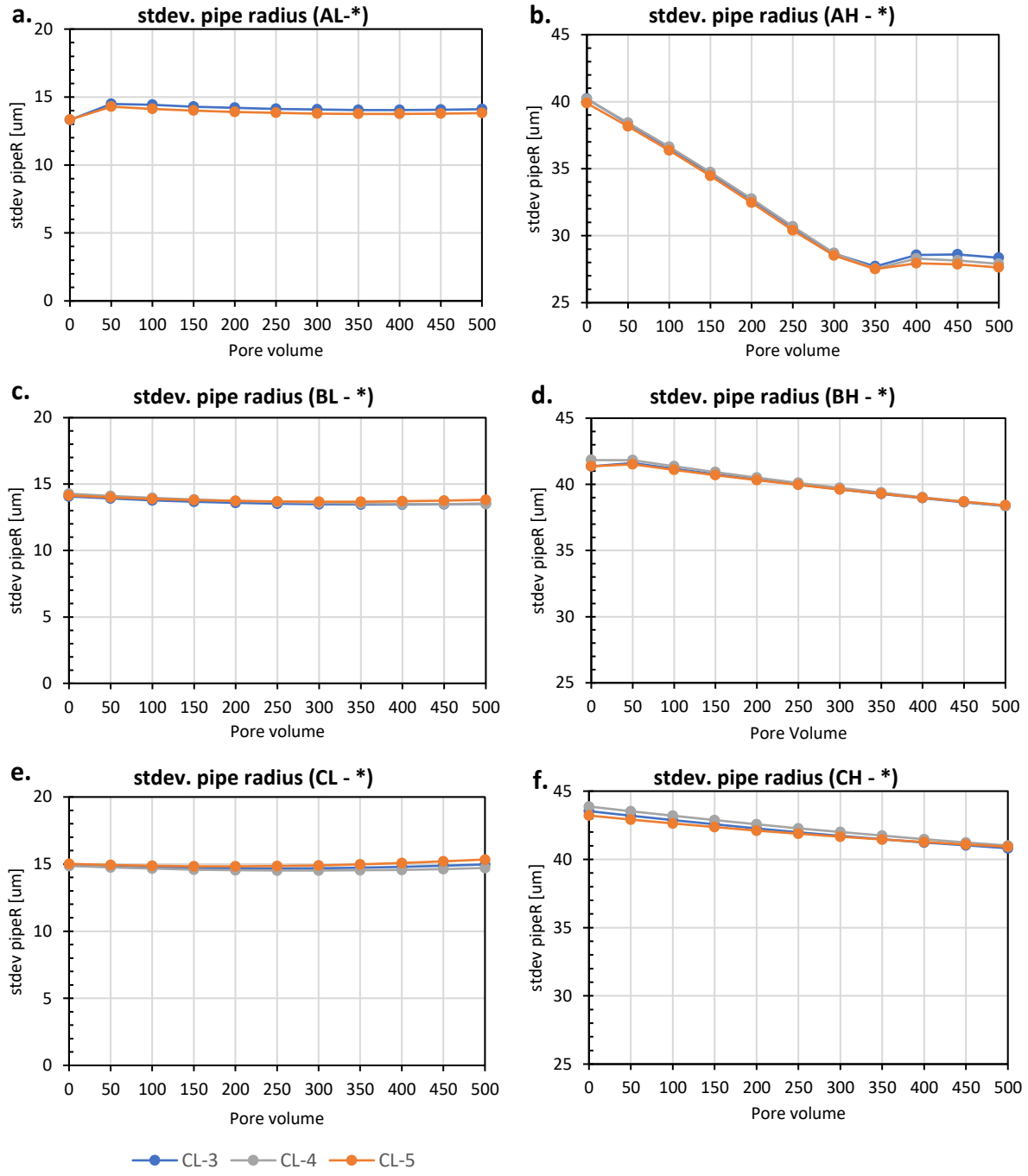

Figure 12
The change in standard deviation of pore-throat radius, over 500 pore volumes (in steps of 50 pore volumes).

Figure 12 shows the change in standard deviation over 500 pore volumes for all networks. Networks with a low initial standard deviation show little change in standard deviation during dissolution, whereas networks with high initial standard deviation all show a decrease in standard deviation. The biggest decrease is seen for network AH-* where the standard deviation decreases almost linearly during the first 350 pore volumes, after which the standard deviation appears relatively constant. Difference in coordination number are again very minimal.

The pore-throat radius evolution is also described in Figure 13 where the distribution at 0, 250 and 500 pore volumes are shown for all networks. Most notable is the change in distribution seen for networks

AL-3 and AH-3. These networks show a right-skewing of the distribution after 250 and 500 pore volumes, which is especially pronounced for network AH-3.

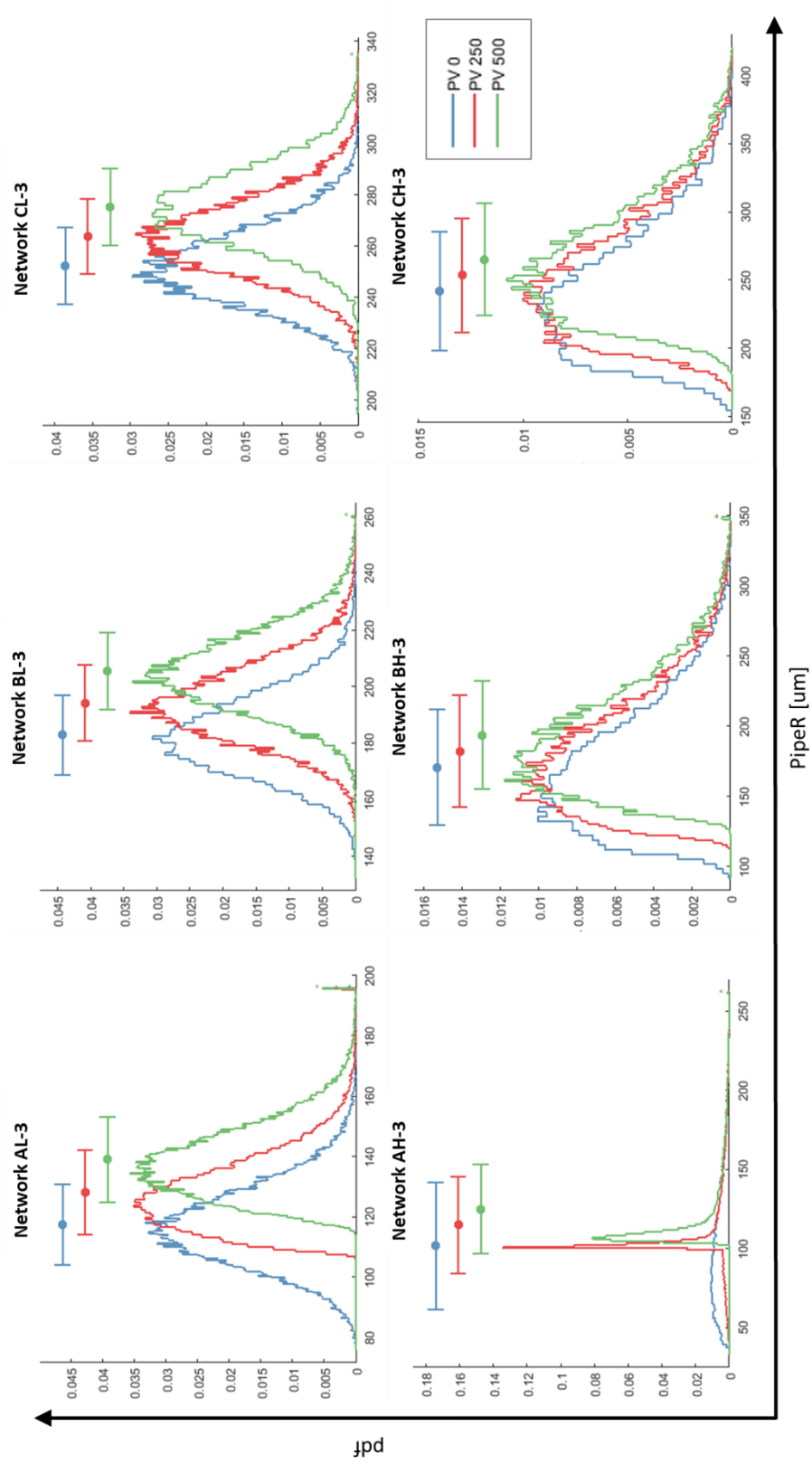

Figure 13
Pore-throat radius distributions after 0, 250 and 500 pore volumes (blue, red and green respectively) for all networks with a coordination number of 3. Shown as a probability density function. Complete set of plots for all networks is given in the Appendix.

The next figure shows the initial distribution of all the residence times for networks with coordination number 5 (i.e. before dissolution). The spread in residence time goes up to 3.1e10 minutes but is most concentrated at much smaller residence times less than 5 minutes. For this reason, the histogram shown here only includes residence times of up 20 minutes and discretizes the smaller residence times into smaller bin sizes. A larger spread can be seen for networks with smaller mean pore-body sizes. Around 80% of residence times are smaller than 0.2 minutes for networks C, 70% for networks B and only 30% for networks A. This indicates that networks with a larger mean have a larger fraction of small residence times.

The average residence time for a range of pore-throat sizes is shown in Figure 15. These results were obtained by truncating the residence time to exclude outliers. The cut-off point was chosen, arbitrarily, as the residence time below which ~95% of the data lies. The figure shows that average residence times seem to be decreasing with increasing pore-throat radius. For networks AL-5 and BH-5, however, the average residence time decreases up to a certain point after which it increases with pore-throat radius. Note, however, that these trends are sensitive to the choice of cut-off point and pore-throat bin sizes.

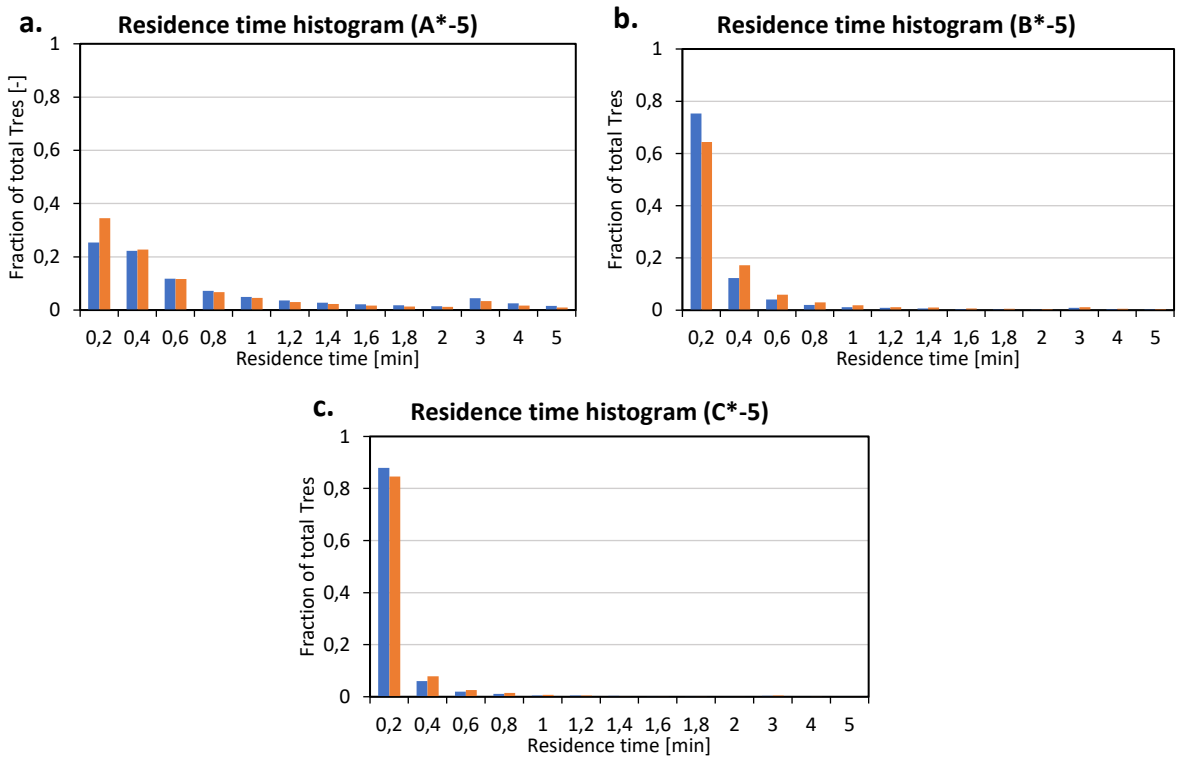

Figure 14

Histogram of residence times for networks A, B and C with an average coordination number 5. Networks with a low initial standard deviation are blue and networks with a high initial standard deviation are orange. Note that not all the data is shown in the histogram and that the bin sizes vary.

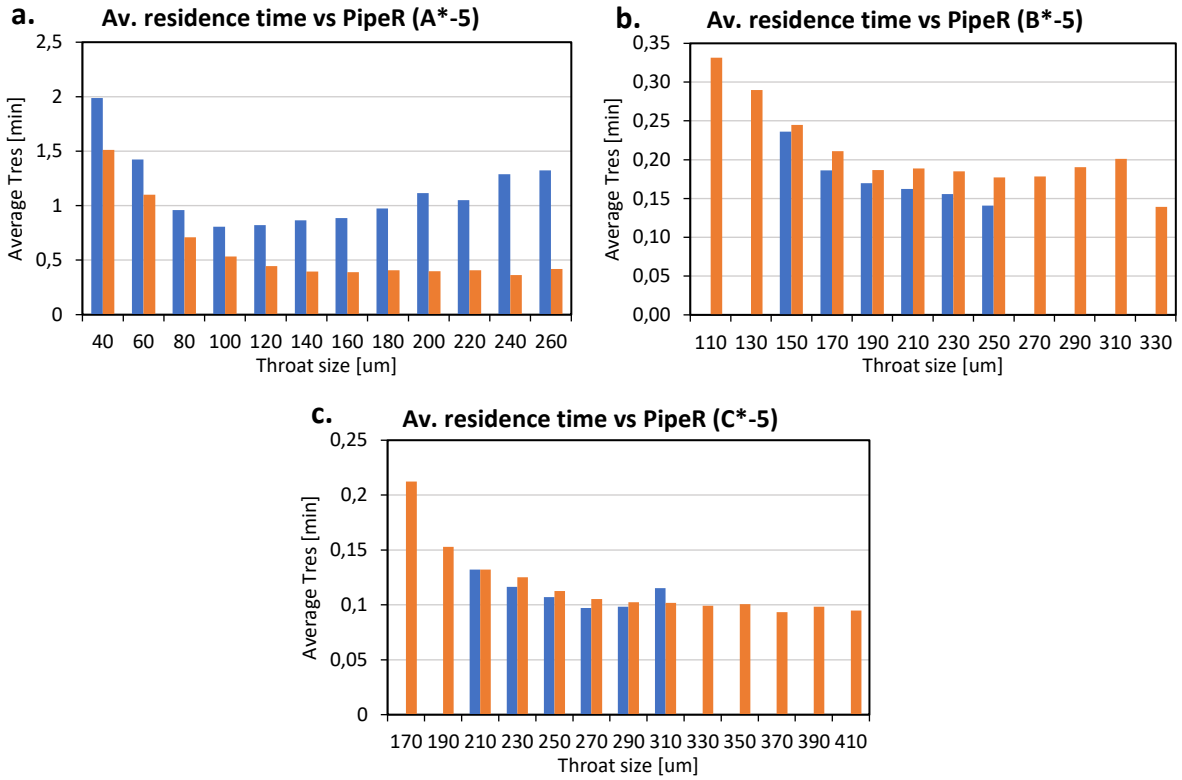

Figure 15

Average residence time for different pore-throat sizes for networks A, B and C and average coordination number 5. Throat sizes are binned and the upper limit of the bin is given on the x-axis. Networks with a low initial standard deviation are coloured blue and networks with a high initial standard deviation are coloured orange.

6 Discussion

With regards to the dissolution behaviour the model shows face dissolution occurring at relatively high velocities (4.82 and 9.63 mm/s). These velocities are much higher than the velocities at which wormholing is commonly reported [e.g. Fredd and Fogler, 1998]. This is interesting seeing as face dissolution is expected to occur at slower velocities than wormholing [Golfier et al., 2001]. In this research, however, the reaction rate is higher due to the high pCO_2 and temperature conditions implemented which causes face dissolution to still occur at relatively high velocities. On the other hand, it is also possible that the reaction rate is overestimated because the rate is assumed here to be reaction-limited whilst the velocities used lie within the range of velocities (0.1 – 1000 cm/s) at which Li et al. (2008) report that mass-transport limitations occur.

To facilitate the analysis of the relative effect of pore-structure parameters, simulations were run at a velocity of 19.2 cm/s to ensure a uniform dissolution. In that way any changes in the parameters could be attributed to dissolution occurring in the entire column rather than only at the inlet. This velocity may seem unrealistically high when considering that a typical groundwater velocity is in the order of m/day (0.001 cm/s). However, because of the earlier mentioned high reactivity of the system uniform dissolution will only occur at a very high velocity whereas a slower groundwater flow velocity would restrict dissolution to the first cell only, which is not practical for the purpose of this study. As mentioned earlier however, it should be noted that in using a velocity of 19.2 cm/s the system may not be considered reaction-limited [Li et al. 2008] and so the rate of dissolution is likely overestimated because this model does not account for the necessary mass-transport limitations. Nonetheless, this issue is not particularly problematic for this research since only the relative effects of the pore-structure parameters are investigated.

For networks with varying initial mean pore-body radii, standard deviation and average coordination number the results show a linear increase in porosity (Figure 9) which is to be expected considering steady-state dissolution is already found after about 1-2 pore volumes (Figure 8a). The differences in rate of porosity increase are related to differences in total surface area, since networks with a larger total surface area will have a faster rate of reaction and will thus also increase in porosity faster. This relation is, to a certain extent, confirmed when comparing differences in rates in Table 4 and differences in total initial surface area in Table 3. Note that the total surface area does evolve over time and that Table 3 thus only gives an indication of what the relative total surface areas are for the different networks. It is found that the rate is higher for networks with a lower mean pore-size, a low standard deviation and/or a coordination number 4, which almost always coincides with a larger initial total surface area seen in Table 3. It makes sense that a lower mean pore size results in a larger total surface area when considering that the surface area to volume ratio is higher for smaller pores and that the density of pores within the fixed network volume will also be larger (more small pores fit into a fixed volume than large pores do). However it is interesting to see that this is still the case despite lower mean-pore sizes having been given a lower porosity. It is important to consider that the effect of pore-size distribution and coordination number on the total surface area is not very intuitive due to the set-up of the simulations. For example, it would usually be expected that a higher coordination number results in a larger number of pore-throats, and thus a larger total surface area of pore-throats and a higher rate of reaction. However, this is not necessarily the case here because the number of nodes for networks with a higher coordination number are lower and the lattice distances larger to ensure they have the same initial porosity value as the other networks with the same pore-size distribution. Together with slight variations in network length and porosity values it then becomes very difficult to determine exactly what the effect of a higher coordination number is on the specific surface area.

Since dissolution is assumed to only occur within pore-throats it is only the pore-throat radius which is affected by dissolution. Interestingly, the coordination number does not seem to affect the evolution of pore-throat distribution parameters (i.e. mean and standard deviation). The mean pore-throat radius is seen to increases linearly for all networks, with the slight exception of networks AL-* and AH-* (Figure 11). Even though dissolution is steady-state (see Figure 8a and 9), this is a somewhat unexpected result. One would actually expect to see the increase in mean pipe radius becoming progressively smaller because pores become less sensitive to pipe radius changes as they increase in radius (Equation 16). As a result of this, differences in pore-sizes also gradually become smaller, but it is only when the network is completely homogeneous, and thus composed of equally sizes pores that increase in radius at the same rate, that the mean pipe radius increases linearly (for a steady-state dissolution). A possible reason for a linear increase in pipe radius in Figure 11 is simply that the range in radius is too small to show the entire curvature. Perhaps if the simulation were run for a longer period, and thus over a larger range in radius, the expected curve could be seen. Unfortunately, it was not possible to carry this out within the time-frame of this research.

In comparing the different networks (Table 5), networks B and C show minimal difference in the rate of increase for the different standard deviations, whereas network A shows much larger variations. For these networks a higher initial standard deviation shows a larger rate of increase than for a lower initial standard deviation. This can again be explained by Equation 16 which shows that the relative increase in pore-throat radius for a given volume of dissolved calcite is much larger for small pores than for large pores. Thus, when considering that a higher standard deviation indicates a larger amount of very small pores this could explain why the initial standard deviation has a larger effect on networks with smaller pore-sizes and why a higher initial standard deviation will show a faster increase in mean pore-throat sizes. Table 5 also shows that the rate of pipe radius increase is higher for networks with a larger mean pore size (i.e. on average, the rate of radius increase for network C is larger than that of network A). This may seem surprising when considering the previous statement, that for a given volume of dissolved calcite small pores should increase in radius more than larger pores. However, it should also be considered that the density of pores is smaller for larger pore-sizes. As a result, the total volume of dissolved calcite will then be distributed over a smaller number of pores, giving each pore a larger volume of calcite to dissolve. This could then compensate for the fact that large pores are less sensitive to radius changes.

With regards to the evolution of the standard deviation of pore-throat radius (Figure 12) a decrease is seen for networks with a high initial standard deviation while remaining almost constant for networks with a low initial standard deviation. This can again be explained by the fact that small pores increase in radius faster than large pores for a given volume of calcite. As such in a network with high standard deviation there are larger variations in pore-sizes and because the small pores will increase in radius faster than large pores this results in a decrease in standard deviation. On the other hand, for networks with a low standard deviation there are little differences in pore-size and so all pores will increase in radius at the same rate which keeps the standard deviation constant. Because the increase in radius is progressively larger for smaller pore-sizes this effect of high standard deviation is much more pronounced for networks with smaller mean pore-sizes.

The evolution of standard deviation can to some degree be related to the distribution of residence time over small and large pores. The residence time is dependent on the size, velocity and configuration of pores and as such it is not intuitive whether the residence time is shorter in smaller pores or in larger pores. If the residence time is the same for all pores, the same volume of calcite is dissolved in every pore. However, this does not result in the same increase in pore-throat radius because small pores will increase more relative to large pores, as previously explained. As such, if the

residence time is the same for all pores the radius of small pores will increase faster than the radius of larger pores, resulting in a decrease in standard deviation. On the other hand, if the residence time is shorter for smaller pores than for larger pores, smaller pores are given a larger volume of calcite to dissolve. As a result, small pores will increase even more relative to large pores and again a decrease in standard deviation will be seen. Finally, if the residence time is shorter for large pores than for small pores, large pores are given a larger volume of calcite to dissolve. One possible result is that larger pores will increase at a faster rate than small pores causing an increase in standard deviation. However, if the difference in residence time is insufficient to outweigh the inherent advantage of small pores small pores could still increase faster than large pores which will again cause a decrease in standard deviation. Another possibility is that a balance is found where the difference in residence time compensates for small pores inherently increasing faster. In this situation the standard deviation would not change. So, from the decrease in standard deviation alone it is not possible to deduce whether it is the small or large pores that have a shorter or longer residence time because a decrease in standard deviation could occur for any of the three possible scenarios. The only situation where any certainty regarding residence times can be expected is when an increase in standard deviation is seen because this is only possible if larger pores have shorter residence times. With this reasoning the initial increase in standard deviation seen for networks AL-* and BH-* (Figure 12) indicate that during the first 50 pore volumes the larger pores have shorter residence times. The histogram in Figure 14 shows a larger fraction of short residence times for networks with a larger mean pore-size which also points to larger pores initially having shorter residence times. However, the initial average residence times for networks AL-* and BH-* (Figure 15) contradict this hypothesis as it shows shortest residence times for intermediate pore-sizes. It should be noted, however, that the distribution of residence time could evolve as the pore-network is evolving and is thus not per se the same after 50 pore volumes. As such a possible explanation could be that the distribution of average residence times has changed during the 50 pore volumes and cannot be coupled with the results seen in Figure 12. There could also be some inaccuracy in the way the figure was obtained as it is quite sensitive to the choice in cut-off point and bin size. Yet another possibility is that the distribution of residence time is much more complicated than initially thought and that short residence times are not exclusively found for small or large pores. Moreover, if the initial increase in standard deviation does in fact indicate large pores have shorter residence times, it would coincide with a wormholing type configuration. In the case of wormholing, channels penetrate the entire column and so velocities are larger for channels with larger radii which gives larger channels a shorter residence time. However, since dissolution is very uniform it seems unlikely that wormholing would occur. This goes to show the complexity in determining the evolution of the network by simply looking at the distribution of the residence time.

7 Conclusion

In this research a coupled reactive transport model is developed which simulates calcite dissolution under CO_2 storage conditions. The model is furthermore implemented for 18 different networks, varying in pore-size distributions and average coordination number, to investigate the relative effects of pore-structure parameters and their evolution during calcite dissolution simulations.
The results are summarized below.

- At relatively high velocities face-dissolution is still occurring, which can in part be explained by an enhanced reactivity induced by the high temperature and pressure conditions but it should also be considered that the rates are possibly overestimated because the velocities used all lie within the range of velocities at which mass-transport is reported to occur [Li Li et al. 2008]. Nonetheless this is not particularly problematic for the analysis of pore-structure parameters as only their relative effects are considered. For this analysis a velocity is chosen at which dissolution occurs uniformly throughout the column (19.2 cm/s).
- When running the model for the various networks the overall dissolution is indeed occurring uniformly throughout the column. However, the calcite concentration in the individual cells does vary significantly per network and thus seems to be quite dependent on the initial network properties.
- As expected for steady-state dissolution a linear increase in porosity is seen in all networks. The rate of increase in porosity is found to increase with decreasing mean pore-size which coincides with higher initial total surface areas found for lower mean pore-sizes. The rate is also found to be higher for networks with a low standard deviation and/or a coordination number of 4, which again coincides with a higher total initial surface area in most cases. However, due to the set-up of network generation it is not very intuitive what exactly the effect is of pore-size distribution and average coordination number on the total surface area of pore-throats.
- The average coordination number does not seem to affect the evolution of pore-throat distribution parameters (i.e. mean and standard deviation) as it only causes minimal differences in results.
- For networks with a small mean pore-size the effect of a high initial standard deviation is much more drastic than for networks with a larger mean pore-size. This is because the increase in pore-throat radius becomes progressively smaller for an increasing pore-size and so small pores increase in radius much faster than large pores. This effect is seen in both the results for the mean and standard deviation of pore-throat radius.
- The mean pore-throat radius is found to increase linearly with pore volume whereas the expectation is that the rate of increase actually gradually diminishes as pores grow larger and become less sensitive to pore-radius changes. A possible explanation could simply be that the range considered is too small to be able to observe this curvature. Furthermore, for networks with a small mean pore-size a high initial standard deviation results in a faster increase in mean pore-throat radius compared to a low initial standard deviation, whereas for networks with a larger mean pore-size the effect of initial standard deviation is minimal. This is caused by the fact that small pores increase in radius faster than large pores. The rate of pore-throat radius increase is also seen to increase with mean pore-size which is explained by the lower density of pores associated for networks with larger mean pore-sizes. A lower density of pores means that the total volume of dissolved calcite is also distributed over less pores, giving the individual pores a larger volume of calcite to dissolve. This thus compensates for the fact that larger pores increase in radius relatively slower than small pores.
- Overall, the standard deviation of pore-throat radius is seen to decrease for networks with high initial standard deviation whereas it remains fairly constant for networks with a low initial standard

deviation. Because the increase in radius varies for different pore-sizes, networks with a larger variation in pore-sizes can be expected to show larger changes in standard deviation. For networks with a small variation in pore-sizes the increase in pore-throat radius can be expected to occur more uniformly. However, because the increase in radius is also dependent on the residence time, it is not clear what the resulting evolution of the network would be.

- A higher fraction of short residence times was found for networks with larger mean pore-sizes.
- For networks showing an initial increase in standard deviation the initial average residence times were found to be shortest for intermediate pore-sizes. This contradicts the hypothesis that residence times must be shorter for larger pores if an increase in standard deviation is seen and indicates that residence times are not only influenced by pore-sizes but are also dependent on specific network configurations. As such it is very difficult to determine the distribution of residence time.

In conclusion, the coupled model developed here shows potential for reactive transport modelling at a modest computational expense. However, further improvements could be made with regards to the reaction rate by incorporation the effect of mass-transfer limitations. With regards to the effect of initial pore-size distribution, networks with small pore-sizes are found to be much more sensitive to dissolution and variations in pore-structure parameters. It is speculated that this is caused by the fact that smaller pores increase in radius much faster than large pores and that it is moreover caused by the fact that small pores have relatively more surface area because of a higher density of pores. Furthermore, there appears to be no clear relationship between the residence-time distribution (i.e. average residence time for a given pore-throat size) and the evolution of the pore-throat distribution which is further evidence of the complexity of the system.

8 References

Acharya, R. C. (2004). *Upcsaling of Nonlinear Reactive Transport: from Pore to Core*. PhD Thesis Wageningen University

Algive, L., Bekri, S., Vizika, O., 2010. Pore-network modeling dedicated to the determination of the petrophysical-property changes in the presence of reactive fluid. SPE J. 15 (03), 618–633.

Ameri, A., Raoof, A., Blonk, C., & Cnudde, V. (2017). Detailed Modeling of Carbonate Acidizing by Coupling a Multi-Purpose Pore-Network Simulator to the Chemistry Package PHREEQC - Application to Chelating Agents. *SPE*. https://doi.org/10.2118/185532-ms

Andreani, M., Luquot, L., Gouze, P., Godard, M., Hoise, E., & Gibert, B. (2009). Experimental study of carbon sequestration reactions controlled by the percolation of CO2-rich brine through peridotites. *Environmental Science and Technology*, *43*(4), 1226–1231. https://doi.org/10.1021/es8018429

Arns, Ji-Youn, Robins, Vanessa, Sheppard, Adrian, Sok, Robert, Pinczewski, W.V, K. M. (2017). *Effect of Network Topology on Relative Permeability*. (February), 21–46. https://doi.org/10.11648/j.pse.20170201.15

Bachu, S., & Adams, J. J. (2003). Sequestration of CO2 in geological media in response to climate change: capacity of deep saline aquifers to sequester CO2 in solution. *Energy Conversion and Management*, *44*(20), 3151–3175. https://doi.org/10.1016/s0196-8904(03)00101-8

Chatzis, I., & Dullien, F. A. L. (1977, January 1). Modelling Pore Structure By 2-D And 3-D Networks With ApplicationTo Sandstones. Petroleum Society of Canada. doi:10.2118/77-01-09

Chou, L., Garrels, R. M., & Wollast, R. (1989). Comparative study of the kinetics and mechanisms of dissolution of carbonate minerals. *Chemical Geology*, *78*(3–4), 269–282. https://doi.org/10.1016/0009-2541(89)90063-6

Dong, H., & Blunt, M. J. (2009). Pore-network extraction from micro-computerized-tomography images. *Physical Review E*, *80*(3), 1–11. https://doi.org/10.1103/PhysRevE.80.036307

Engineering ToolBox, (2004). *Water - Dynamic and Kinematic Viscosity*. [online] Available at: https://www.engineeringtoolbox.com/water-dynamic-kinematic-viscosity-d_596.html [Accessed 18-06-2019].

Fredd, C. N., & Scott Fogler, H. (1998). Influence of transport and reaction on wormhole formation in porous media. *AIChE Journal*, *44*(9), 1933–1949. https://doi.org/10.1002/aic.690440902

Golfier, F., Bazin, B., Zarcone, C., Lernormand, R., Lasseux, D., & Quintard, M. (2001). Acidizing Carbonate Reservoirs: Numerical Modelling of Wormhole Propagation and Comparison to Experiments. *SPE-68922*.

Gunter, W. D., Bachu, S., Law, D. H.-S., Marwaha, V., Drysdale, D. L., Macdonald, D. E., & McCann, T. J. (1996). Technical and economic feasibility of CO2 disposal in aquifers within the Alberta sedimentary basin, Canada. *Energy Conversion and Management*, *37*(6–8), 1135–1142. https://doi.org/10.1016/0196-8904(95)00311-8

IPCC, 2013: Climate Change 2013: The Physical Science Basis. Contribution of Working Group I to the Fifth Assessment Report of the Intergovernmental Panel on Climate Change [Stocker, T.F., D. Qin, G.-K. Plattner, M. Tignor, S.K. Allen, J. Boschung, A. Nauels, Y. Xia, V. Bex and P.M. Midgley (eds.)]. Cambridge University Press, Cambridge, United Kingdom and New York, NY, USA, 1535

Kim, D., Peters, C., Lindquist, W., 2011. Upscaling geochemical reaction rates accompanying acidic CO2-saturated brine flow in sandstone aquifers. Water Resources Research 47 (1).

Koutsoukos, P., Kontoyannis, C., 1984. Precipitation of calcium carbonate in aqueous solutions. Journal of the Chemical Society Faraday Transactions 1 80 (5), 1181–1192.

Kovscek, A. R., & Wang, Y. (2005). Geologic storage of carbon dioxide and enhanced oil recovery. I. Uncertainty quantification employing a streamline based proxy for reservoir flow simulation. *Energy Conversion and Management*, *46*(11–12), 1920–1940. https://doi.org/10.1016/j.enconman.2004.09.008

Li, L., Peters, C. A., & Celia, M. A. (2006). Upscaling geochemical reaction rates using pore-scale

network modeling. *Advances in Water Resources*, *29*(9), 1351–1370. https://doi.org/10.1016/j.advwatres.2005.10.011

Li, L., Steefel, C. I., & Yang, L. (2008). Scale dependence of mineral dissolution rates within single pores and fractures. *Geochimica et Cosmochimica Acta*, *72*(2), 360–377. https://doi.org/10.1016/j.gca.2007.10.027

Mehmani, Y., Sun, T., Balhoff, M. T., Eichhubl, P., & Bryant, S. (2012). Multiblock Pore-Scale Modeling and Upscaling of Reactive Transport: Application to Carbon Sequestration. *Transport in Porous Media*, *95*(2), 305–326. https://doi.org/10.1007/s11242-012-0044-7

Morse, J. W., & Arvidson, R. S. (2002). The dissolution kinetics of major sedimentary carbonate minerals. *Earth Science Review*, *58*, 51–84. https://doi.org/10.1016/S0012-8252(01)00083-6

Nelson, P. H. (2009). *Pore-throat sizes in sandstones , tight sandstones , and shales*. *93*(3), 329–340. https://doi.org/10.1306/10240808059

Nogues, J. P., Fitts, J. P., Celia, M. A., & Peters, C. A. (2013). Permeability evolution due to dissolution and precipitation of carbonates using reactive transport modeling in pore networks. *Water Resources Research*, *49*(9), 6006–6021. https://doi.org/10.1002/wrcr.20486

Noiriel, C., Luquot, L., Mad, B., Raimbault, L., Gouze, P., Van Der Lee, J., 2009. Changes in reactive surface area during dissolution process: an experi- mental and modelling study. Chemical Geology 265 (1-2), 160–170.

Parkhurst, B. D. L., & Appelo, C. A. J. (1999). User's Guide To Phreeqc (Version 2)— A Computer Program For Speciation, and Inverse Geochemical Calculations, Water-Resources Investigations Report 99-4259, Denver, CO. *Water-Resources Investigations Report*, (Version 2). https://doi.org/Rep. 99-4259

Parkhurst, D. L., & Appelo, C. A. J. (2013). Description of Input and Examples for PHREEQC Version 3--A Computer Program for Speciation, Batch-Reaction, One-Dimensional Transport, and Inverse Geochemical Calculations. *U.S. Geological Survey Techiniques and Methods*, *book 6*(chap. A43), 497. https://doi.org/10.1016/0029-6554(94)90020-5

Parkhurst, D. L., Thortenson, D. C., & Plummer, L. N. (1980). PHREEQE-A computer program for geochemical calculations. In *US Geological Survey Water Resources Investigations*.

Plummer, L. N., & Busenberg, E. (1982). The solubilities of calcite, aragonite, and vaterite in carbon dioxide-water solutions between 0 and 90°C, and an evaluation of the aqueous model for the system calcium carbonate-carbon dioxide-water. *Geochimica et Cosmochimica Acta*, *46*(6), 1011–1040. https://doi.org/10.1016/0016-7037(82)90056-4

Plummer, L. N., Wigley, T. M. L., & Parkhurst, D. L. (1978). The kinetics of calcite dissolution in CO2-water systems at 5 to 60 degrees C and 0.0 to 1.0 atm CO2. *American Journal of Science*, *278*(2), 179–216. https://doi.org/10.2475/ajs.278.2.179

Ramharack, R., Aminian, K. and Ameri, S. (2010). *Impact of Carbon Dioxide Sequestration in Gas/Condensate Reservoirs*. SPE Eastern Regional Meeting.

Raoof, A., & Hassanizadeh, S. M. (2010). Upscaling Transport of Adsorbing Solutes in Porous Media. *Journal of Porous Media*, *13*(5), 395–408. https://doi.org/10.1615/jpormedia.v13.i5.10

Raoof, A., & Majid Hassanizadeh, S. (2009). A new method for generating pore-network models of porous media. *Transport in Porous Media*, *81*(3), 391–407. https://doi.org/10.1007/s11242-009-9412-3

Raoof, A., Nick, H. M., Hassanizadeh, S. M., & Spiers, C. J. (2013). PoreFlow: A complex pore-network model for simulation of reactive transport in variably saturated porous media. *Computers and Geosciences*, *61*, 160–174. https://doi.org/10.1016/j.cageo.2013.08.005

Raoof, A., Nick, H. M., Wolterbeek, T. K. T., & Spiers, C. J. (2012). Pore-scale modeling of reactive transport in wellbore cement under CO2 storage conditions. *International Journal of Greenhouse Gas Control*, *11*(SUPPL), S67–S77. https://doi.org/10.1016/j.ijggc.2012.09.012

Rochelle, C., Czernichowski-Lauriol, I. and Milodowski, A. (2004). *The impact of chemical reactions on CO2storage in geological formations: a brief review*. Geological Society, London, Special Publications, 233(1), pp.87-106.

Sjöberg, E. L. (1978). Kinetics and mechanism of calcite dissolution in aqueous solutions at low

temperatures. *Stockholm Contributions in Geology*, *32*, 92.
Solomon, S., Plattner, G.-K., Knutti, R., & Friedlingstein, P. (2009). Irreversible climate change due to carbon dioxide emissions. *Proceedings of the National Academy of Sciences of the United States of America*, *106*(6), 1704–1709. https://doi.org/10.1073/pnas.0812721106
Stocker, T. F., & Schmittner, A. (1997). Influence of carbon dioxide emission rates on the stability of the thermohaline circulation. *Nature*, *388*(August), 862–865.
Thomas, C. J. (2000). Causes of Climate Change Over the Past 1000 years. *Science*, *289*(July), 270–277. https://doi.org/10.1126/science.289.5477.270
Varloteaux, C., Békri, S., Adler, P.M., 2013. Pore network modelling to determine the transport properties in presence of a reactive fluid: from pore to reservoir scale. Advances in Water Resources 53, 87-100.

Appendix

Contents

1 Main executable (script)

```
@echo off
setlocal enabledelayedexpansion


REM             ###  GENERAL DESCRIPTION ###
REM This batch file includes the code to run the 1D reactive transport model. The model uses two existing models,
REM PoreFlow and PHREEQC, to achieve this. Each model is in its own directory, in which they have their respective
REM input and output files. The input PoreFlow requires from PHREEQC is the amount of kinetically dissolved
REM calcite, which is found in the text file delCalcite.txt. The input PHREEQC requires from PoreFlow is the
REM average radius and total area of each segment of the pore structure, which is found in PHREEQC_CELL_INFO.TXT.
REM Lines 15-116 are the code used for the initialization of the model, creating/generating the necessary initial
REM input files. The lines thereafter actually run the model for the desired number of timesteps given in line 18.


REM 1. User prompt for number of timesteps and initial
::-------------------------------------------------------------------------
echo.
set /p x=Enter number of timesteps:
echo.
set /p initial_moles=Enter initial number of moles of calcite per segment:


REM 2. Choose pore size distribution
REM m = mean (200/300/400um)
REM s = stdev (30/87um for m=200 and 30/86 for m=300/400)
REM c = coord. nr. (3/4/5)
::-----------------------------------------------------
set m=200
set s=30
set c=5

echo.
echo                ************************************
echo                RUNNING PORE SIZE DISTRIBUTION WITH:
echo                mean = %m%
echo                stdev = %s%
echo                coordination nr. = %c%
echo                ************************************
echo.


REM 3. Clear input and results folder from previous run
::-----------------------------------------------------
del /f/q phreeqc\CSV\*
del /f/q phreeqc\*
del /f/q poreflow\RESULTS\SELECTED_OUTPUT\*
del /f/q poreflow\RESULTS\*
del /f/q poreflow\INPUTS

REM 4. Copy initial phreeqc input files to input folder
::-----------------------------------------------------------------
cd phreeqc\Initial_input_phreeqc
copy /y * ..\..\phreeqc
cd ..\..\poreflow\INPUTS\mean_%m%\stdev_%s%\coordnr_%c%\Initial
copy /y initial_porosities1.txt ..\..\..\..\..\..\phreeqc


REM 5. Copy initial PoreFlow input files to input folder
REM and set run counter to 0 for initial run
::-----------------------------------------------------------------

REM Copy initial delCalcite (zero) from phreeqc to poreflow INPUTS
cd ..\..\..\..\..\..\phreeqc
copy /y delCalcite_initial.txt ..\poreflow\INPUTS\delCalcite.txt
REM Copy all specific network files to INPUTS
cd ..\poreflow\INPUTS\mean_%m%\stdev_%s%\coordnr_%c%\Initial
copy /y * ..\..\..\..\..\..\INPUTS

REM Copy poreflow input file (for a user defined network) into the working input file
cd ..
copy /y nettype2.in ..\..\..\..\INPUTS\poreflow.in

REM Set run_counter to zero
cd ..\..\..\..\INPUTS
echo 0 > poreflow_run_counter.txt


REM 6. Run PoreFlow to create initial PHREEQC_CELL_INFO
REM and copy it to the phreeqc input folder
::-----------------------------------------------------
cd ..\PoreFlow\PoreFlow
call poreflow_win10

REM Copy inital PHREEQC_CELL_INFO to phreeqc input
cd ..\..\RESULTS
copy /y PHREEQC_CELL_INFO.TXT ..\..\phreeqc
::-----------------------------------------------------


REM 7. Copy initial conditions for phreeqc to dump files which will
REM be used in PHREEQC with the INCLUDE$ keyword.
REM The dump files will be overwritten with every run!
::-------------------------------------------------------------------
cd ..\..\phreeqc
copy /y initial_dump1.dmp dump.dmp
copy /y initial_trans1.dmp trans.dmp
copy /y initial_porosities1.txt porosities.txt
REM copy /y initial_porosities.txt porosities.txt !!


REM 8. Creating KINETIC datablock and appending to it the parameters from PHREEQC_CELL_INFO
::-------------------------------------------------------------------------------------------

REM Creating KINETIC datablock for each cell (no values for parameters yet!)
REM This is done in Batch because when done in PHREEQC as: KINETICS 1-20... the k_modify (created below) does not
REM modify the KINETICS data block for all the cells properly, which is necessary to include the initial average
REM radius and total surface area of each segment of the pore structure. As such the KINETICS data block, created
REM in Batch, is appended to the dump.dmp file which already includes the initial SOLUTION data block. This is all
REM done in the subroutine ":kinetics_datablock", with the first argument being the initial number of moles of calcite.
call :kinetics_datablock %initial_moles%

```

```
REM Create k_modify.txt (which will include the parameters for the above KINETICS data blocks). k_modify.txt will be
REM included in the phreeqc input file using INCLUDE$, essentially modifying the above KINETICS data block with the
REM necessary parameters (radius, area) from PoreFlow (i.e.PHREEQC_CELL_INFO.TXT).
REM See subroutine ":kinetics_modify" at the end of this file!
call :kinetics_modify


REM 9. Starting loop over timesteps
::-------------------------------------------------------------------------------------------------------------------------
echo.
echo ================================================
echo ============STARTING REACTIVE TRANSPORT=============
echo ================================================

REM Now that the initialization has been done, we run PHREEQC and PoreFlow for every timestep; first PHREEQC then PoreFlow.
REM looping over number of timesteps
for /l %%i in (1, 1, %x%) do (
    echo.
    echo ---------------TIMESTEP %%i----------------

    REM Appending porosity and total cell volume to PHREEQC_CELL_INFO
    call :selected_output 1 "porosities.txt" "PHREEQC_CELL_INFO"
    echo   1543 >> "PHREEQC_CELL_INFO.TXT"
    REM !!! average Vtot !!!

    REM RUN PHREEQC
    call phreeqc Phrqc_diff.pqi


    REM update m0 such that it is equal to the amount of calcite left after the previous timestep, otherwise it will go back to 10 moles by default
    echo. > k_modify.txt
        for /l %%j in (1, 1, 20) do (
        echo KINETICS_MODIFY %%j >> k_modify.txt
        echo INCLUDE$ PHREEQC_CELL_INFO.TXT >> k_modify.txt
        set /a line=0
        for /F "tokens=1 usebackq" %%G in ("delCalcite.txt") do (
        set /a line+=1
        set /a p=%%j+21
        if !line! EQU !p! (
        echo -m0    %%G >> "k_modify.txt")
        )
        echo. >> k_modify.txt
    )

    REM Copy porosities calculated in phreeqc to porosities.txt
    echo -porosities > porosities.txt
    set /a line=0
    for /F "tokens=* usebackq" %%G in ("porosities_full.txt") do (
        set /a line+=1
        if !line! GTR 21 (
        echo %%G >> "porosities.txt")
        )

    REM Create CSV files to be viewed in ParaView; pH and Calcite. This is done using subroutine ":create_csv"
    call :create_csv %%i "pH_temp.txt" "pH_0" "pH_1" "pH_%%i"
    call :create_csv %%i "delCalcite.txt" "Calcite_0" "Calcite_1" "Calcite_%%i"
    call :create_csv %%i "solution.txt" "Solution_0" "Solution_1" "Solution_%%i"
    call :create_csv %%i "porosities_full.txt" "por_0" "por_1" "por_%%i"

    REM Copy output from phreeqc to poreflow input file
    copy /y delCalcite.txt ..\poreflow\INPUTS

    REM RUN POREFLOW
    cd ..\poreflow\PoreFlow\PoreFlow
    call poreflow_win10

    cd ..\..\INPUTS
    copy /y Qij.TXT ..\RESULTS\Qij_%%i.TXT

    REM copy PHREEQC_CELL_INFO.TXT to phreeqc input directory
    cd ..\RESULTS
    copy /y PHREEQC_CELL_INFO.TXT ..\..\phreeqc

    REM REM update porosities file for phreeqc
    REM echo -porosities > porosities.txt
    REM set /a line=0
    REM for /F "tokens=6 usebackq" %%G in ("INFO_0.TXT") do (
    REM set /a line+=1
    REM set /a b=%%i+2
    REM if !line! EQU !b! (
    REM echo %%G >> "porosities.txt")
    REM )
    REM copy /y porosities.txt ..\..\phreeqc

    REM change back to phreeqc directory
    cd ..\..\phreeqc

)


REM 10. Copy porosity/permeability data for each timestep from INFO_0.txt into seperate files
::-------------------------------------------------------------------------------------------------------------------------
cd ..\poreflow\RESULTS
call :selected_output 6 "INFO_0.txt" "SELECTED_OUTPUT\porosity"
call :selected_output 4 "INFO_0.txt" "SELECTED_OUTPUT\conductivity"

exit /b

::------------------------------------------- END -----------------------------------------------
```

```
REM 11. Subroutines
::-------------------------------------------------------------------------------------------
REM Subroutine to create kinetics datablock
:kinetics_datablock
for /l %%i in (1, 1, 20) do (
```

```
    echo. >> dump.dmp
    echo KINETICS %%i >> dump.dmp
    echo Calcite >> dump.dmp
    echo -tol   1e-8 >> dump.dmp
    echo -bad_step_max 50000 >> dump.dmp
    REM Following line includes the initial amount of calcite
    echo -m0    %1 >> dump.dmp
    echo -m     %1 >> dump.dmp
    echo -parms >> dump.dmp
)
exit /b
REM Subroutine to create kinetics_modify.txt
:kinetics_modify
echo. > k_modify.txt
REM loop over number of cells\segments
for /l %%i in (1, 1, 20) do (
    echo KINETICS_MODIFY %%i >> k_modify.txt
    REM line to include output file from PoreFlow
    echo INCLUDE$ PHREEQC_CELL_INFO.TXT >> k_modify.txt
    echo. >> k_modify.txt
)
exit /b
REM Subroutine to extract initial surface activities and copy them to PHREEQC_CELL_INFO
:ini_surfact_to_PCI
echo ################################### >> %~2
echo #surface_activity %~3 >> %~2
echo ################################### >> %~2
FOR /l %%i IN (1,1,20) DO (
    set /a line=0
    FOR /F "tokens=%4 usebackq" %%G IN ("%~1") DO (
        set /a line+=1
        IF !line! GTR %5 (
        echo %%G >> "%~2")
    )
)
exit /b
REM Subroutine to extract surface activities during run and copy them to PHREEQC_CELL_INFO
:surfact_to_PCI
echo ################################### >> %~2
echo #surface_activity %~3 >> %~2
echo ################################### >> %~2
set /a line=0
FOR /F "tokens=%4 usebackq" %%G IN ("%~1") DO (
    set /a line+=1
    IF !line! GTR %5 (
        echo %%G >> "%~2")
)
exit /b
REM Subroutine to create CSV files
:create_csv
if %1==1 (
    set /a line=0
    for /F "tokens=* usebackq" %%G in ("%~2") do (
        set /a line+=1
        if !line! LEQ 21 if !line! GTR 1 (
            echo %%G >> "CSV\%~3.csv")
        if !line! GTR 21 (
            echo %%G >> "CSV\%~4.csv")
    )
) else (
    set /a line=0
    for /F "tokens=* usebackq" %%G in ("%~2") do (
        set /a line+=1
        if !line! GTR 21 (
            echo %%G >> "CSV\%~5.csv")
    )
)
exit /b
REM Subroutine to create files for selected_output (e.g. porosity and conductivity)
:selected_output
for /F "tokens=%1 skip=1 usebackq" %%G in ("%~2") do (
    echo %%G >> "%~3.txt"
)
exit /b
REM The following code is from Stephen Knight (2012), Dragon Computer Consulting
REM ========================================
REM Subroutines to calculate run time are below
REM ========================================
:START
set start=%date% %time:~0,8%
REM echo START at %start%
exit /b

:END
set end=%date% %time:~0,8%
REM echo END at %end%
exit /b

:ShowDiff
REM Call with s,n,h for seconds, mins, hours. defaults to secs
(set type=%~1)& if "%~1"=="" set type=s

echo Wscript.Echo DateDiff("%type%", #%start%#,#%end%# ) > "%temp%\timediff.vbs"
for /f %%s in ('cscript //nologo "%temp%\timediff.vbs"') do set TimeDiff=%%s
del "%temp%\timediff.vbs"
if %Type%==n set type=m
echo TOTAL TIME TAKEN: %TimeDiff% %Type%
exit /b

endlocal
```

2 Network generating executable (script)

```
@echo off
setlocal enabledelayedexpansion


REM               ###  GENERAL DESCRIPTION ###
REM In this batch file PoreFlow is implemented to generate an initial pore-network for a specified
REM pore size distribution and coordination number. These initial pore-networks are later used in the coupled model!
REM The pore geometry input files needed for the coupled model are created here, and are saved to a specific folder for
REM the specified mean, stdev and coordination number. Pore size distributions are pre-defined and were made assuming a
REM lognormal distribution for a range of different mean and stdev.


REM 1. Choose pore size distribution
REM m = mean (200/300/400um)
REM s = stdev (30/87um for m=200 and 30/86 for m=300/400)
REM c = coord. nr. (3/4/5)
::-----------------------------------------------------
set m=200
set s=30
set c=4

echo.
echo                ====================================
echo                RUNNING PORE SIZE DISTRIBUTION WITH:
echo                mean = %m%
echo                stdev = %s%
echo                coordination nr. = %c%
echo                ====================================
echo.


REM 2. Clear results folder and initial phreeqc input
::-----------------------------------------------------
del /f/q poreflow\RESULTS\*
del /f/q poreflow\INPUTS\*
del /f/q poreflow\INPUTS\mean_%m%\stdev_%s%\coordnr_%c%\Initial\*


REM 3. Copy initial input files into poreflow INPUTS folder
::-----------------------------------------------------------
REM Initial delCalcite (zero)
cd phreeqc
copy /y delCalcite_initial.txt ..\poreflow\INPUTS\delCalcite.txt
REM Specified pore distribution (as PORER.TXT) and run_counter
cd ..\poreflow\INPUTS\mean_%m%\stdev_%s%
copy /y m%m%s%s%.txt ..\..\..\INPUTS\PORER.TXT
REM PoreFlow input file (for random network generator)
cd coordnr_%c%
copy /y nettype1.in ..\..\..\..\INPUTS\poreflow.in


REM 4. Run PoreFlow to generate random network for coupled model
::---------------------------------------------------------------
cd ..\..\..\..\PoreFlow\PoreFlow
call poreflow_win10


REM 5. Copy (and rename) necessary results to initial inputs folder
::-----------------------------------------------------------------------------------
cd ..\..\RESULTS
copy /y PORER_0.TXT ..\INPUTS\mean_%m%\stdev_%s%\coordnr_%c%\Initial\PORER.TXT
copy /y PIPEL_0.TXT  ..\INPUTS\mean_%m%\stdev_%s%\coordnr_%c%\Initial\PIPEL.TXT
copy /y PIPER_0.TXT ..\INPUTS\mean_%m%\stdev_%s%\coordnr_%c%\Initial\PIPER.TXT
copy /y PIPER_0.TXT ..\INPUTS\mean_%m%\stdev_%s%\coordnr_%c%\Initial\PIPER_INITIAL.TXT
copy /y Qij_0.TXT ..\INPUTS\mean_%m%\stdev_%s%\coordnr_%c%\Initial\Qij_INITIAL.TXT
copy /y INFO_0.TXT ..\INPUTS\mean_%m%\stdev_%s%\coordnr_%c%\Initial\INFO_INITIAL.TXT
copy /y CONF.TXT ..\INPUTS\mean_%m%\stdev_%s%\coordnr_%c%\Initial
copy /y PORE_LOC.TXT ..\INPUTS\mean_%m%\stdev_%s%\coordnr_%c%\Initial
copy /y PORE_INLET.TXT ..\INPUTS\mean_%m%\stdev_%s%\coordnr_%c%\Initial
copy /y LIST.DAT ..\INPUTS\mean_%m%\stdev_%s%\coordnr_%c%\Initial


REM 6. Copy initial porosity to initial_porosities1.txt (20x), which will be used in the coupled model
::-------------------------------------------------------------------------------------------------------
cd ..\INPUTS\mean_%m%\stdev_%s%\coordnr_%c%\Initial
echo -porosities > initial_porosities1.txt

for /l %%i IN (1, 1, 20) do (
set /a line=0
for /F "tokens=6 usebackq" %%G in ("INFO_INITIAL.TXT") do (
    set /a line+=1
    if !line! GTR 1 (
    echo %%G >> "initial_porosities1.txt")
    )
)




endlocal
```

3 PHREEQC input file

```
#########################################################################
# 1D kinetic dissolution model of calcite due to low pH solution injection
# Naod Negash and Flor Wassing
# 15-04-2019
#########################################################################

#Create injection solution with pure water in equilibrium with CO2
SOLUTION 0 Injection fluid in eq. with CO2 #such that pH~3.5
    temp      50
    pH        7 charge
    pe        4
    redox     pe
    units     mol/kgw
    density   1
    -water    1 # kg
EQUILIBRIUM_PHASES 0
    CO2(g)    2 10 # pCO2 = 10^1 atm = 10 MPa
SAVE SOLUTION 0
END


#Reading SOLUTION 1-20 and KINETICS 1-20 from dump.dmp
#Initially the dump.dmp include SOLUTION and KINETICS datablocks but will be rewritten to a _RAW format after the first run.
INCLUDE$ dump.dmp

#Include k_modify.txt which modifies each KINETICS datablock to include the parameters in PHREEQC_CELL_INFO.TXT. The file
#PHREEQC_CELL_INFO.TXT consists of a list of parameters for each cell (i.e. first 20 are the average pipe radius, next 20 are
#average pipe length etc.)
INCLUDE$ k_modify.txt

#The following RATES datablock includes our rate equation for calcite dissolution. Basic lines 1 and 2 read the average radius and
#total reactive surface area for each cell from the parameters defined in PHREEQC_CELL_INFO.TXT.

RATES
Calcite
 -start
1   R = PARM(CELL_NO)                       #average radius for cell [m]
2   A = PARM(CELL_NO+40)                    #total reactive surface area [m^2]

# Rate constants at 50 C, calculated from Arrhenius equation:
# Ea from Plummer et al. 1978 and k25C from Chou et al. 1989 to find A values
10  k1 = 1.16                               #rate constant mol/m2/s (Chou et al., 1989)
20  k2 = 1.85*10^(-3)                       #"
30  k3 = 1.85*10^(-6)                       #"
40  Ksp = 10^LK_PHASE("Calcite")            #equilibrium constant calcite [-] (PHREEQC database)

50 Rate = (k1*ACT("H+") + k2*ACT("CO2") + k3)*(1 - (ACT("CO3-2")*ACT("Ca+2")/Ksp))
60 moles = Rate * A * TIME

140 Vtot = PARM(101)                                            #Total volume of a cell (as per PoreFlow, determined externally); [mm3]
141 ini_por = PARM(CELL_NO+80)                                  #Starting porosity [-]
142 IF(TOTAL_TIME=0) THEN Vf = ini_por*Vtot ELSE Vf=GET(1,cell_no)  #Total fluid volume (Vf); [mm3]
143 dmol=(M0-M)                                                 #Define the amount of dissolved calcite to calculate the porosity change
144 delcal = dmol * (Vf / 1000000)                              #Amount of dissolved calcite adjusted for the volume of a cell in PoreFlow [moles]
145 molmass = 100.0869                                         #molar mass of calcite; [g/mol]
146 dens = 2.711                                               #density of calcite; [g/cm3]
147 dV = (delcal * (molmass/dens))*1000                        #Volume of dissolved calcite; times by 1000 to get cm3 in mm3 [mm3]
148 dPor = dV/Vtot                                             #Change in porosity; change in volume over total volume
149 new_por = ini_por + dPor                                   #New porosity [-]
150 CHANGE_POR(new_por,cell_no)                                #Changing porosity to new porosity
151 Vf=new_por*Vtot
152 PUT(Vf,1,cell_no)

100 SAVE moles
 -end


#Reading TRANSPORT datablock from trans.dmp
INCLUDE$ trans.dmp
INCLUDE$ porosities.txt

USER_PUNCH 1
-headings k_Calcite  dk_Calcite
-start
10 PUNCH M
20 PUNCH M-M0
-end

USER_PUNCH 4
-headings -porosities
-start
10 PUNCH GET_POR(CELL_NO)
-end


#Dumping new solution composition and kinetic data in _RAW format (-.dmp is overwritten)
DUMP
-file dump.dmp
-append false
-solution 1-20
-kinetics 1-20

#Output the amount of kinetically dissolved/precipitated calcite to delCalcite.txt, which is used as input for PoreFlow. This file
#will also serve as a source for the creation of CSV files to track the development of amount of calcite in each cell, allowing it
#to be viewed in ParaView.
SELECTED_OUTPUT 1
    -file                delCalcite.txt
    -high_precision      true
    -user_punch          true
    -reset               false
    -time                false
    -step                false
    -solution            false


#Output the pH in each cell, used for the generation of CSV files to view pH development in the network over time.
SELECTED_OUTPUT 2
    -file           pH_temp.txt
    -high_precision true
    -reset          false
    -solution       false
```

```
    -pH             true

SELECTED_OUTPUT 3
-file            solution.txt
-high_precision true
-reset           false
-molalities      H+ Ca+2 OH- CO3-2 CO2 HCO3-


SELECTED_OUTPUT 4
    -file               porosities_full.txt
    -high_precision     true
    -user_punch         true


END
```

4 Initial_dump (PHREEQC initial solution datablock)

```
SOLUTION 200 Background solution in eq. with calcite #initially filling column
    temp      50
    pH        7 charge
    pe        4
    redox     pe
    units     mol/kgw
    density   1
    -water    1 # kg
EQUILIBRIUM_PHASES 200
    Calcite 0 # SI(Calcite) = 0
SAVE SOLUTION 1-20
END # not including this END statement affects results!
```

5 Initial_trans (PHREEQC transport datablock)

```
TRANSPORT
# total column length = lengths x cells
# velocity = lengths/time_step
# dispersivity = 0.1 x lengths
    -cells                20
    -shifts               250 #per 12.5 pore volumes
    -time_step            0.025 # seconds
    -lengths              0.004816# meter
    -dispersivities       0.0004816
    -print_cells          1-20
    -punch_cells          1-20
    -punch_frequency      250
    -multi_d              true 1e-09 0.15 0 1
```

6 PoreFlow input file for network generation (Network AL-3)

```
*** BLOCK A: SIMULATION MODE ****************************************
***SIMULATION MODE: 1: ONLY NET GEN, 2:NET+FLOW, 3:NET+FLOW+TRANSPORT, 4:NET+FLOW+REACTIVE TRANSPORT
SIMMODE
2
*** BLOCK B: NETWORK TYPE ****************************************
***NETTYPE: 1:RANDOM NETWORK, 2:USER DEFINED NETWORK
NETTYPE
1
*** BLOCK B: NETWORK PARAMETERS ****************************************
***NETTYPE: 1:RANDOM NETWORK, 2:USER DEFINED NETWORK
Ni  Nj  Nk Ncont
113    22   22    850.d0
***NETTYPE: 1:RANDOM NETWORK, 2:USER DEFINED NETWORK
COORDINATION_NUMBER
avgCoordination dirTreshNums
.true.    .false.
3.0
***DIRRECTION_THRESHOLD_NUMBERS
***0.7462    0.7462    0.7462    0.7462    0.7462    0.7462    0.7462    0.7462    0.7462   0.7462   0.7462    0.7462    0.7462
***NETTYPE: PORE SIZE CALCULATION
PORESIZE_CALCULATION
readBodySizes,    readtThroatSizes, readPipelSizes,  readBodyVolumes, readThroatVolumes, pipelEnhancedByPorer, lengthUnit
.true.          .false.          .false.          .false.          .false.          .true.               um
*** BLOCK C: FLOW BC ****************************************
***FLOW DIRECTION: xFlowToRight, xFlowToLeft, yFlowIntoPlabe, yFlowOutofPlabe, zFlowToTop, zFlowToBottom
FLOW_DIRECTION
xFlowToRight, xFlowToLeft, yFlowIntoPlabe, yFlowOutofPlabe, zFlowToTop, zFlowToBottom, inletBndThicknessFactor, outletBndThicknessFactor
.true.    .false.  .false.  .false.  .false.  .false. 1.0 1.0
***NETTYPE: PORE THROAT CALCULATION (needed only is readtThroatSizes is .false.)
THROAT_CALCULATION
pipeRadiusCof
0.3d0
*** BLOCK C: FLOW PARAMETERS ****************************************
***VISCOSITY, DENSITY
FLUID1
VISCOSITY DENSITY
0.0005    1000
*** BLOCK C: FLOW TYPE ****************************************
***FLOWBCMODE: CONSTANT PRESSURE, CONSTANT FLUX:  prInlet, {prOutlet, peTarget}
FLOWTYPE
1
*** BLOCK C: FLOW BC ****************************************
***FLOWBCMODE: CONSTANT PRESSURE, CONSTANT FLUX:  prInlet, {prOutlet, peTarget}
prInlet prOutlet
10    0
***NETTYPE: EXCHANGE WITH 'PHREEQC'
PHREEQC_OUTPUT_000
nPhreeqcCell, PhreeqcCellSize[mm], rho_Calcite[mol/mm3], startPhrqLine, startPhrqColm, calciteMult, corCoef, upperCutOverMean, piperMaxAfterDiss
20            4.8025              0.000027             22             2             1.0           1.0      10000.0          0.1
*** BLOCK D: TRANSPORT PARAMETERS ****************************************
***Dmol***
SOLUTE_COMPONENT_PROPERTIES
nSolComp    nSolidComp   poreThroatOnlyFlag  Dmol          lDiff,      transportMode
1           0            .false.          60.00D-5      2.0         2
*** BLOCK D: COMP. NAMES ****************************************
SOLUTE_COMPONENT_NAME
solute1
*** BLOCK D: TRANSPORT BC ****************************************
***'1_Hplus',      '2_HCO3',     '3_H2CO3',       '4_CO3',        '5_Ca',    '6_CaHCO3',        '7_OH',      '8_CaOH',       '9_CO2',        '10_CaCO3'
SOLUTE_COMPONENT_BC
1.0
*** BLOCK D: TRANSPORT IC ****************************************
***'1_Hplus',      '2_HCO3',     '3_H2CO3',       '4_CO3',        '5_Ca',    '6_CaHCO3',        '7_OH',      '8_CaOH',       '9_CO2',        '10_CaCO3'
SOLUTE_COMPONENT_INITIAL
0
*** BLOCK F: SIMULATION TIME PARAMETERS ****************************************
SIMULATION_TIME
timeStopCriterions, pvStopCriterions,  porosiyValueStopCriterions, porosiyChangeStopCriterions
    0        1        0        0
1
MAIN
*** BLOCK F: SIMULATION TIME PARAMETERS ****************************************
TIMESTEP
initialTimeIndex DtMultiplier   DtMaxVal userRectionStepSizeOn userRectionStepSizeVal
0 100D0    0.1D0   .false.  0.1
*** BLOCK F: OUTPUT PARAMETERS ****************************************
OUTPUT_CONTROL
DesiredDataRecord
50
ENDPOREFLOW
```

7 PoreFlow input file for coupled model (Network AL-3)

```
*** BLOCK A: SIMULATION MODE ****************************************
***SIMULATION MODE: 1: ONLY NET GEN, 2:NET+FLOW, 3:NET+FLOW+TRANSPORT, 4:NET+FLOW+REACTIVE TRANSPORT
SIMMODE
2
*** BLOCK B: NETWORK TYPE ****************************************
***NETTYPE: 1:RANDOM NETWORK, 2:USER DEFINED NETWORK
NETTYPE
2
*** BLOCK B: NETWORK PARAMETERS ****************************************
***NETTYPE: 1:RANDOM NETWORK, 2:USER DEFINED NETWORK
Ni  Nj  Nk Ncont
113    22   22    850.d0
***NETTYPE: 1:RANDOM NETWORK, 2:USER DEFINED NETWORK
COORDINATION_NUMBER
avgCoordination dirTreshNums
.true.    .false.
3.0
***DIRRECTION_THRESHOLD_NUMBERS
***0.7462    0.7462    0.7462    0.7462    0.7462    0.7462    0.7462    0.7462    0.7462   0.7462   0.7462    0.7462    0.7462
***NETTYPE: PORE SIZE CALCULATION
PORESIZE_CALCULATION
readBodySizes,    readThroatSizes, readPipelSizes,  readBodyVolumes, readThroatVolumes, pipelEnhancedByPorer, lengthUnit
.true.        .true.          .true.          .false.          .false.          .false.               um
*** BLOCK C: FLOW BC ****************************************
***FLOW DIRECTION: xFlowToRight, xFlowToLeft, yFlowIntoPlabe, yFlowOutofPlabe, zFlowToTop, zFlowToBottom
FLOW_DIRECTION_000
xFlowToRight, xFlowToLeft, yFlowIntoPlabe, yFlowOutofPlabe, zFlowToTop, zFlowToBottom, inletBndThicknessFactor, outletBndThicknessFactor
.true.    .false.  .false.  .false.  .false.  .false. 1.0 1.0
***NETTYPE: PORE THROAT CALCULATION (needed only is readtThroatSizes is .false.)
THROAT_CALCULATION
pipeRadiusCof
0.3d0
*** BLOCK C: FLOW PARAMETERS ****************************************
***VISCOSITY, DENSITY
FLUID1
VISCOSITY DENSITY
0.0005    1000
*** BLOCK C: FLOW TYPE ****************************************
***FLOWBCMODE: CONSTANT PRESSURE, CONSTANT FLUX:  prInlet, {prOutlet, peTarget}
FLOWTYPE
1
*** BLOCK C: FLOW BC ****************************************
***FLOWBCMODE: CONSTANT PRESSURE, CONSTANT FLUX:  prInlet, {prOutlet, peTarget}
prInlet prOutlet
10    0
***NETTYPE: EXCHANGE WITH 'PHREEQC'
PHREEQC_OUTPUT
nPhreeqcCell, PhreeqcCellSize[mm], rho_Calcite[mol/mm3], startPhrqLine, startPhrqColm, calciteMult, corCoef, upperCutOverMean, piperMaxAfterDiss
20           4.8025              0.000027             22             2              1.0           1.0      10000.0          0.1
*** BLOCK D: TRANSPORT PARAMETERS ****************************************
***Dmol***
SOLUTE_COMPONENT_PROPERTIES
nSolComp    nSolidComp   poreThroatOnlyFlag  Dmol           lDiff,      transportMode
1           0            .false.             60.00D-5       2.0         2
*** BLOCK D: COMP. NAMES ****************************************
SOLUTE_COMPONENT_NAME
solute1
*** BLOCK D: TRANSPORT BC ****************************************
***'1_Hplus',      '2_HCO3',      '3_H2CO3',       '4_CO3',        '5_Ca',    '6_CaHCO3',        '7_OH',      '8_CaOH',       '9_CO2',        '10_CaCO3'
SOLUTE_COMPONENT_BC
1.0
*** BLOCK D: TRANSPORT IC ****************************************
***'1_Hplus',      '2_HCO3',      '3_H2CO3',       '4_CO3',        '5_Ca',    '6_CaHCO3',        '7_OH',      '8_CaOH',       '9_CO2',        '10_CaCO3'
SOLUTE_COMPONENT_INITIAL
0
*** BLOCK F: SIMULATION TIME PARAMETERS ****************************************
SIMULATION_TIME
timeStopCriterions, pvStopCriterions,  porosiyValueStopCriterions, porosiyChangeStopCriterions
    0        1        0        0
1
MAIN
*** BLOCK F: SIMULATION TIME PARAMETERS ****************************************
TIMESTEP
initialTimeIndex DtMultiplier   DtMaxVal userRectionStepSizeOn userRectionStepSizeVal
0 100D0    0.1D0   .false.  0.1
*** BLOCK F: OUTPUT PARAMETERS ****************************************
OUTPUT_CONTROL
DesiredDataRecord
50
ENDPOREFLOW
```

8 Initial pore-sizes (PORER, PIPER and PIPEL)

Pore Radius				
Network	*Mean [um]*	*Stdev [um]*	*Min [um]*	*Max [um]*
AL-3	200	30	119	360
AH-3	199	87	55	410
AL-4	200	30	119	360
AH-4	199	87	55	410
AL-5	200	30	119	360
AH-5	199	87	55	410
BL-3	300	30	207	446
BH-3	300	86	151	505
BL-4	300	30	207	446
BH-4	300	86	151	505
BL-5	300	30	207	446
BH-5	300	86	151	505
CL-3	400	30	289	520
CH-3	400	86	250	600
CL-4	400	30	289	520
CH-4	400	86	250	600
CL-5	400	30	289	520
CH-5	400	86	250	600

Pipe Radius				
Network	*Mean [um]*	*Stdev [um]*	*Min [um]*	*Max [um]*
AL-3	117	13	76	205
AH-3	102	40	33	260
AL-4				
AH-4				
AL-5	117	13	76	188
AH-5	102	40	32	261
BL-3	183	14	132	251
BH-3	171	41	92	327
BL-4	183	14	132	257
BH-4	171	42	92	325
BL-5	183	14	137	248
BH-5	170	41	91	330
CL-3	252	15	195	315
CH-3	242	44	154	399
CL-4	253	15	203	324
CH-4	241	44	154	397
CL-5	252	15	195	308
CH-5	241	43	155	399

Pipe Length				
Network	*Mean [um]*	*Stdev [um]*	*Min [um]*	*Max [um]*
AL-3	117	13	76	205
AH-3	102	40	33	260
AL-4				
AH-4				
AL-5	117	13	76	188
AH-5	102	40	32	261
BL-3	183	14	132	251
BH-3	171	41	92	327
BL-4	183	14	132	257
BH-4	171	42	92	325
BL-5	183	14	137	248
BH-5	170	41	91	330
CL-3	252	15	195	315
CH-3	242	44	154	399
CL-4	253	15	203	324
CH-4	241	44	154	397
CL-5	252	15	195	308
CH-5	241	43	155	399

9 Change in standard deviation of PipeR

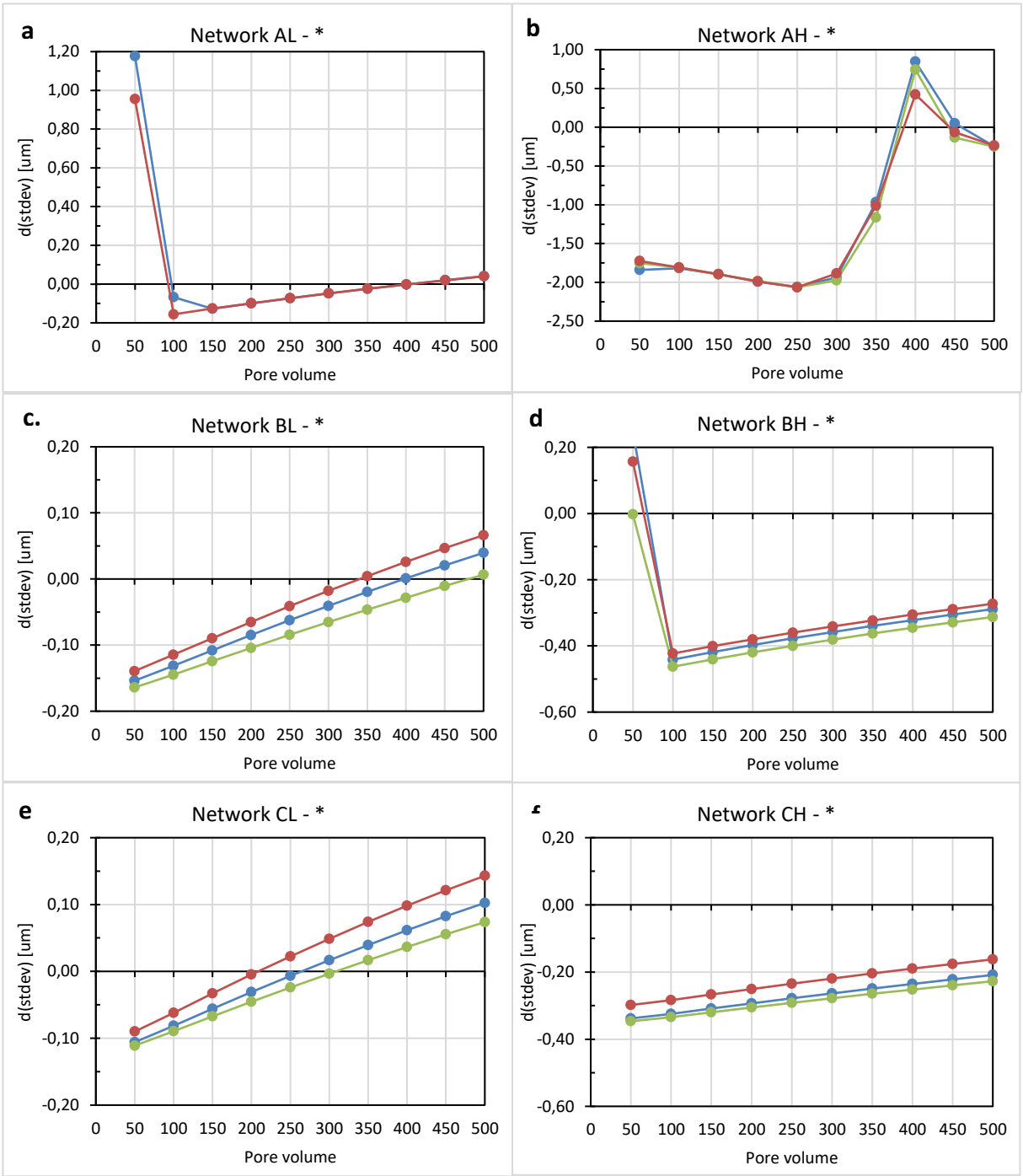

The change in standard deviation of pore-throat radius, over 500 pore volumes (in steps of 50 pore volumes). Colours blue, green and purple indicate coordination numbers 3, 4 and 5 respectively.

10 Mean pore-throat radius for networks B and C

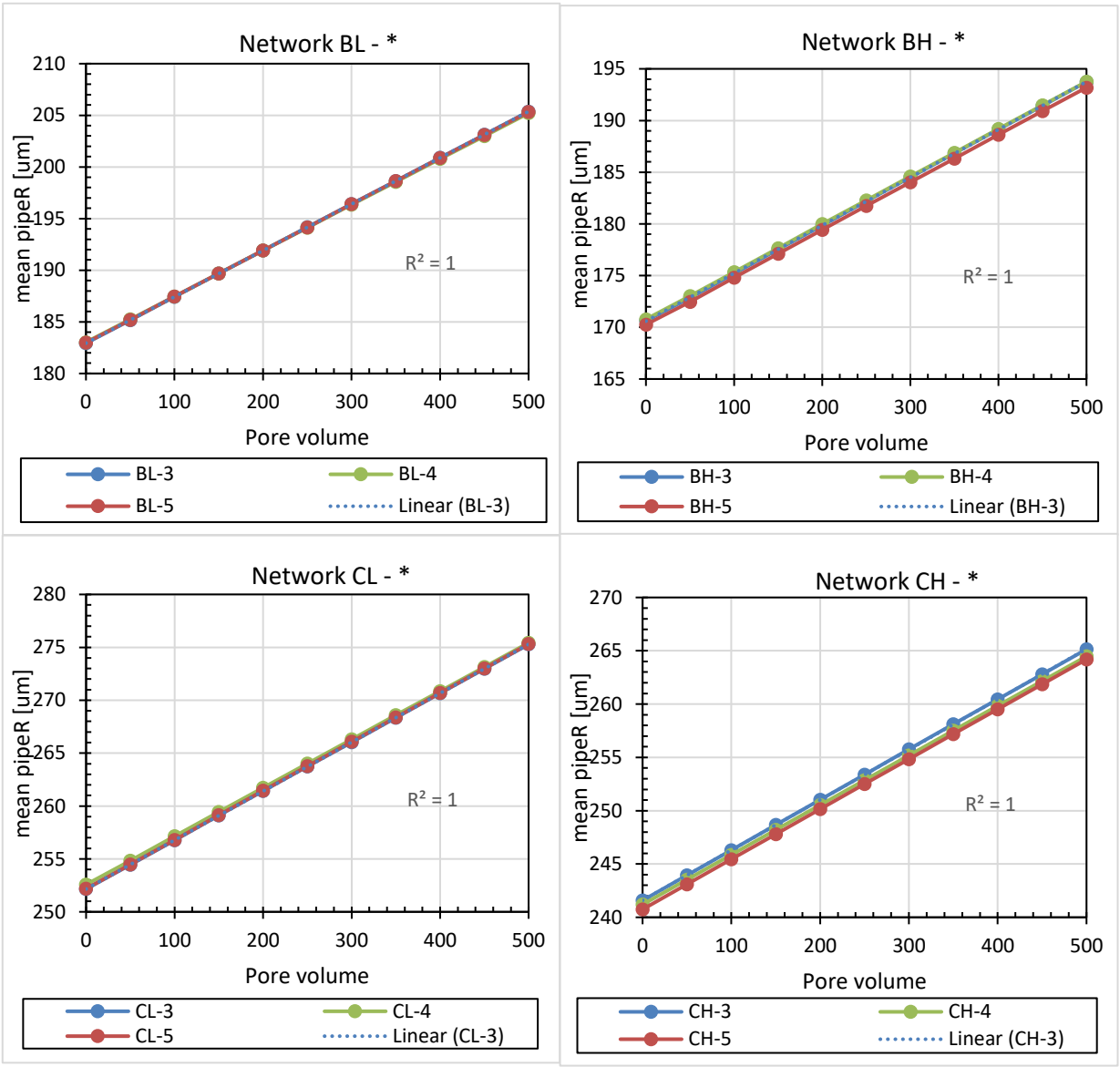

11 Pore-size distribution for network A

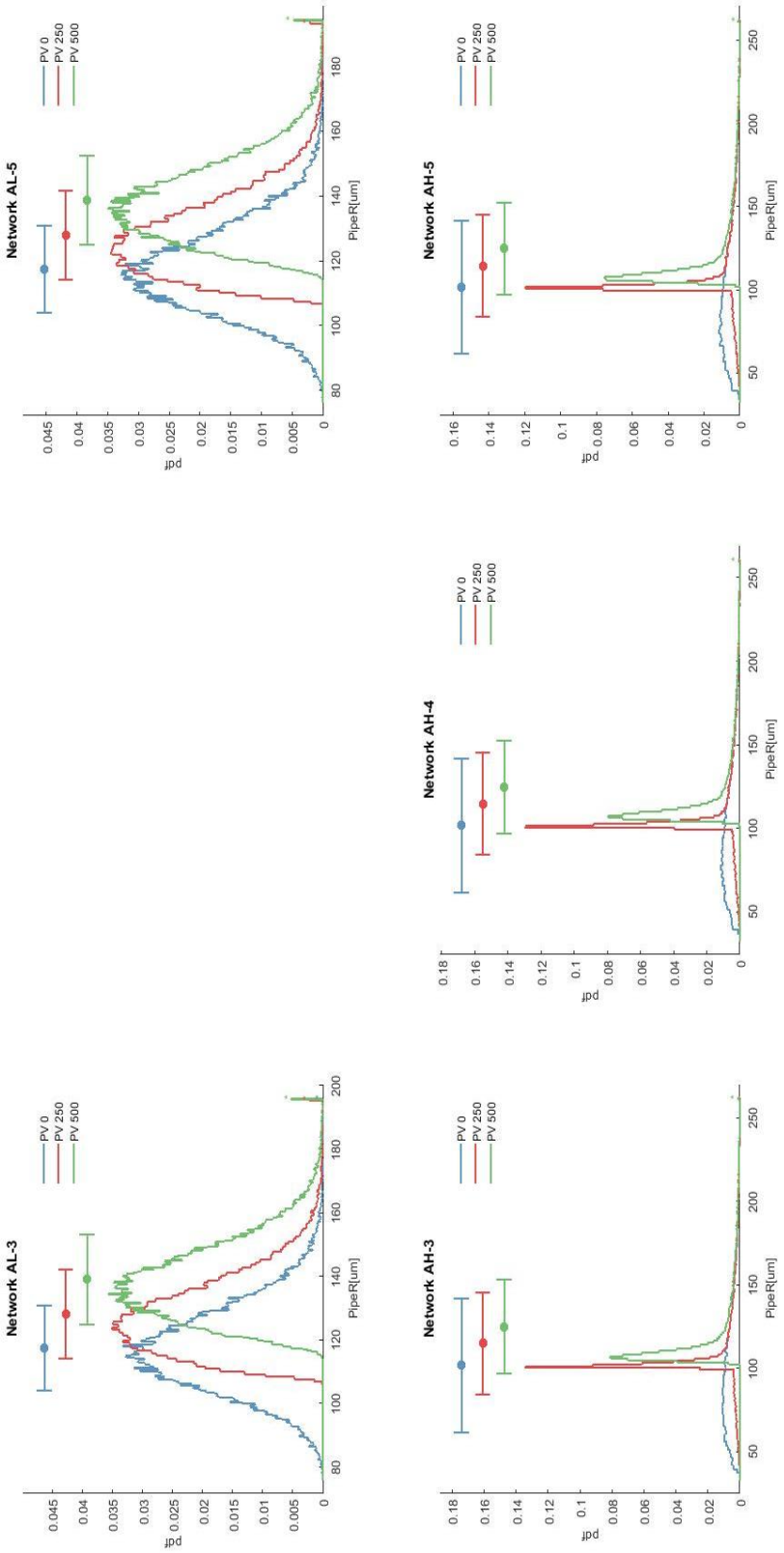

12 Pore-size distribution of network B

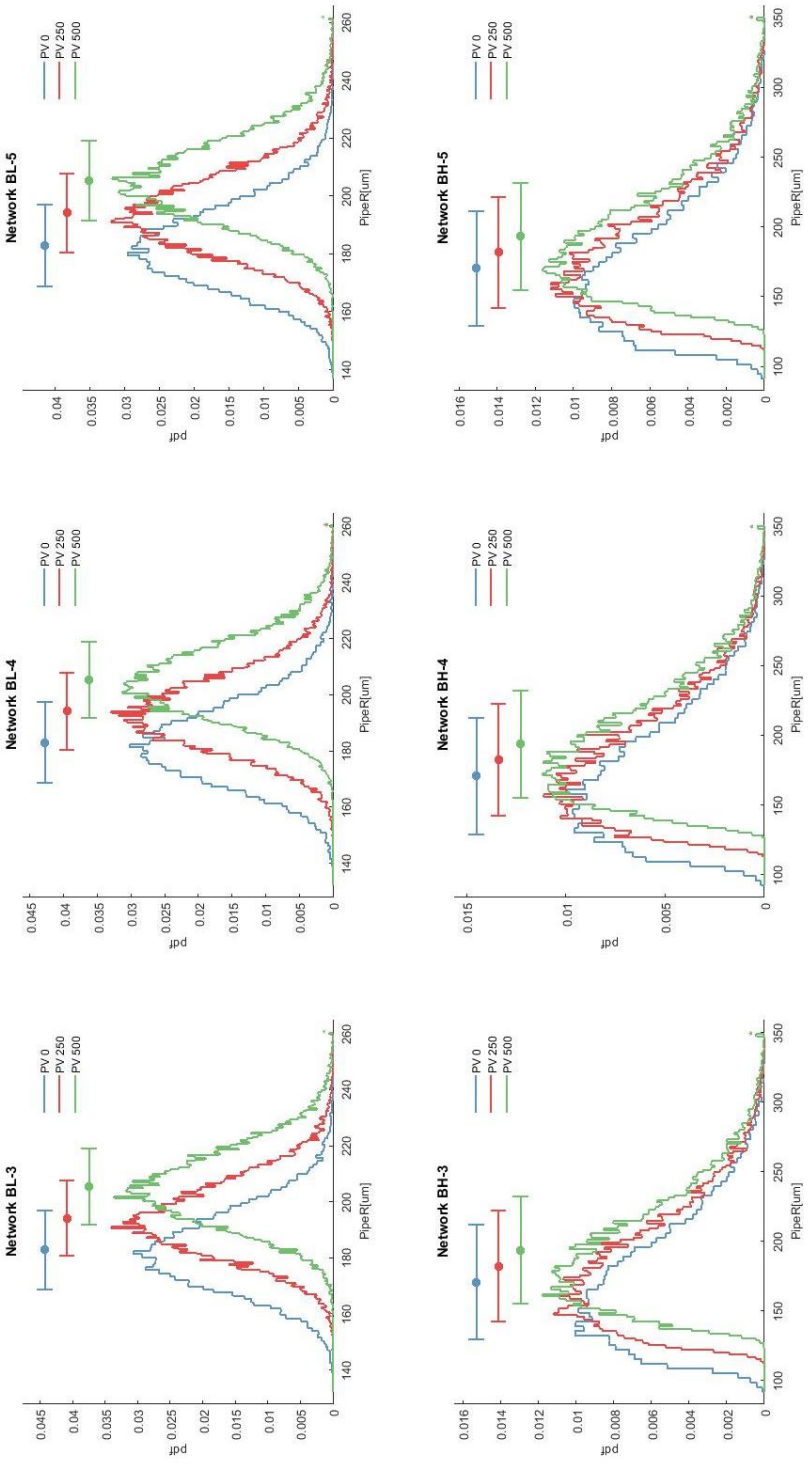

13 Pore-size distribution network C

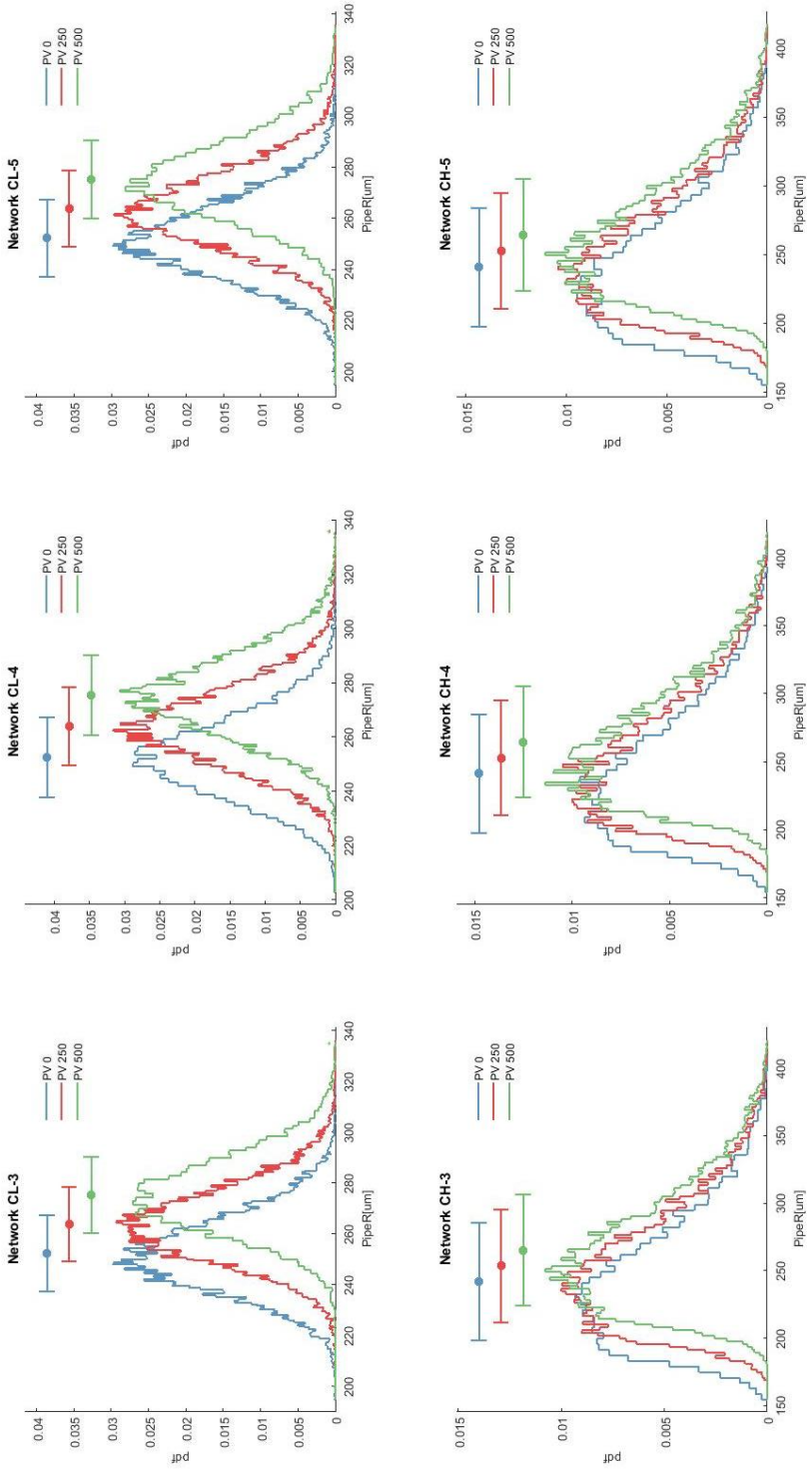

14 Comparing coupling interval